Rectifying Conductance Substates in a Large Conductance Ca^{2+}-activated K^+ Channel: Evidence for a Fluctuating Barrier Mechanism

GUY W. J. MOSS and EDWARD MOCZYDLOWSKI

From the Department of Pharmacology and Department of Cellular and Molecular Physiology, Yale University School of Medicine, New Haven, Connecticut 06520

ABSTRACT In this study, we investigated the mechanism underlying the production of inwardly rectifying subconductance states induced in large conductance Ca^{2+}-activated K^+ channels (maxi K(Ca) channels) by the small, homologous proteins, bovine pancreatic trypsin inhibitor (BPTI) and dendrotoxin-I (DTX). Low-resolution bilayer recordings of BPTI-induced substates display excess noise that is well described by a β-distribution characteristic of a filtered, two-state process. High-resolution patch recordings of maxi K(Ca) channels from vascular smooth muscle cells confirm that the BPTI-induced substate is actually comprised of rapid, voltage-dependent transitions between the open state and a nearly closed state. Patch recordings of DTX-induced substates also exhibit excess noise consistent with a similar two-state fluctuation process that occurs at rates faster than those measured for the BPTI-induced substate. The results indicate that these examples of ligand-induced substates originate by a fluctuating barrier mechanism that is similar to one class of models proposed by Dani, J. A., and J. A. Fox (1991. *J. Theor. Biol.* 153:401–423) to explain subconductance behavior of ion channels. To assess the general impact of such rapid fluctuations on the practical measurement of unitary currents by amplitude histograms, we simulated single-channel records for a linear, three-state scheme of C(closed)-O(open)-S(substate). This simulation defines a range of transition rates relative to filter frequency where rapid fluctuations can lead to serious underestimation of actual unitary current levels. On the basis of these experiments and simulations, we conclude that fluctuating barrier processes and open channel noise may play an important physiological role in the modulation of ion permeation.

INTRODUCTION

Dendrotoxins from mamba snake venom are a family of ~60 residue proteins containing three conserved disulfide bonds that externally block certain isoforms of voltage-sensitive K^+ channels (K_V channels) with nanomolar affinity (Harvey and Anderson, 1985; Hurst et al., 1991). Kunitz inhibitor proteins are a distinct class of serine protease inhibitors that are found in numerous vertebrate tissues and plasma (Creighton and Charles, 1987). They occur as small ~58-residue proteins (e.g., bovine pancreatic trypsin inhibitor, BPTI) and as distinct domains of larger proteins (e.g., inter-α-trypsin inhibitor). Kunitz protease inhibitors are structurally homologous to dendrotoxins (Skarzynski, 1992) with ~30% identity, but are ineffective as extracellular blockers of K_V channels (Marshall and Harvey, 1992). Similarly, dendrotoxins are weak inhibitors of trypsin and kallikrein (Marshall and Harvey, 1990). In contrast to these activities, both dendrotoxin-I (DTX) and BPTI inhibit maxi K(Ca) channels from the internal side, by inducing the appearance of discrete subconductance events (Lucchesi and Moczydlowski, 1990, 1991). This paper concerns the mechanism by which this latter subconductance behavior is produced.

Previous work showed that the DTX/BPTI interaction with the maxi K(Ca) channels obeys kinetics expected for reversible binding at a single class of sites; i.e., substate durations are independent of concentration (first-order dissociation) and the dwell time between adjacent substate events varies inversely with concentration (bimolecular association) (Lucchesi and Moczydlowski, 1990, 1991). The substate durations are well resolved with a mean dwell time of ~0.2 s for BPTI and ~11 s for DTX at 0 mV. Thus, this ligand-channel interaction resembles "slow block" of K^+ channels by Ba^{2+} and charybdotoxin (Vergara and Latorre, 1983;

Address correspondence to Dr. Guy Moss, Department of Pharmacology, Yale University School of Medicine, Sterling Hall of Medicine, 333 Cedar Street, New Haven, CT 06520-8066.

J. GEN. PHYSIOL. © The Rockefeller University Press • 0022-1295/96/01/47/22 $2.00
Volume 107 January 1996 47–68

Miller et al., 1985); however, the substates themselves are reminiscent of a "fast block" (Hille, 1992). This latter analogy is based on the reduced unitary conductance and the inwardly rectifying substate *I-V* curve, in contrast to the relatively ohmic *I-V* relation of the unmodified maxi K(Ca) channel. Unlike true fast block of K channels by an organic cation such as tetraethylammonium (TEA), the level of the substate current induced by DTX and BPTI does not decrease with increasing inhibitor concentration. Furthermore, the observed substate current level varies for different structural homologues of DTX or BPTI (Moczydlowski et al., 1992; G. W. J. Moss and E. Moczydlowski, unpublished results). These results suggest that binding of these inhibitors somehow modifies the energetics of K^+ permeation through the channel.

From a theoretical standpoint, changes in unitary channel conductance can arise by a variety of mechanisms (Dani and Fox, 1991). One class of mechanisms involves electrostatic changes in the channel mouth or vestibule. If the vestibule is partially occluded by a charged ligand, or if negative surface charges in the vestibule are neutralized by a ligand, this may lead to a reduction in unitary current by perturbation of ion–ion interactions or a decrease in the effective concentration of permeant cations at the channel entrance (e.g., Schild and Moczydlowski, 1994). However, the DTX/BPTI subconductance behavior is not competitive with internal pore blockers such as TEA and Ba^{2+}, and the substate is not relieved by increased ionic strength (Lucchesi and Moczydlowski, 1991). This implies that the binding site(s) for BPTI and DTX is not located within the inner vestibule of the K(Ca) channel and argues that surface electrostatics are not involved.

Other possible mechanisms for the production of channel substates involve conformational changes of the channel protein (Dani and Fox, 1991). For example, binding of a ligand may induce a long-lasting change in the structure of the open channel from one conformation to another, resulting in a less favorable free energy profile for ion permeation with an intrinsically lower conductance. Alternatively, the structure of the channel protein may spontaneously fluctuate on a rapid time scale between a high-conductance conformation and a low-conductance conformation. In this case, a change in apparent conductance can occur if binding of a ligand to the channel alters the equilibrium between these two states. Since single-channel recordings are invariably filtered by the recording system, a particular observed current level may actually correspond to the filtered average of many rapidly fluctuating protein conformations (Läuger, 1983, 1985; Andersen et al., 1986).

In this study, we have identified which of these latter two classes of conformational mechanisms accounts for the DTX/BPTI subconductance phenomenon. By using β-function analysis of excess noise (Yellen, 1984), we find that BPTI- and DTX-induced substates arise from a dynamic process involving rapid current fluctuations. In the case of BPTI, we used high resolution patch recordings of maxi K(Ca) channels in aortic smooth muscle cells to ascertain that the apparent substate is actually due to fast, voltage-dependent fluctuations between the open state and a very low conductance state. To generalize our findings, we developed a computer simulation of a simple C(closed)-O(open)-S(substate) process to determine the effect of fast fluctuations on practical measurements of unitary currents as routinely carried out with the use of amplitude histograms. This simulation identifies a border region beyond which rapid transition rates relative to filter frequency lead to an underestimation of the underlying unitary current amplitude. The simulations and actual recordings of DTX-induced substates demonstrate that the amplitude of excess current noise is not always a reliable indication of whether standard histogram measurements reflect the true open-channel current. The simulations also illustrate cases in which apparent changes in channel gating and unitary current can be manifestations of a change in one pair of rate constants. Application of these results to analysis of subconductance behavior and open-channel rectification is discussed in reference to related work on open-channel noise and fluctuating barrier mechanisms. Preliminary reports of this work have been published in abstract form (Moss and Moczydlowski, 1993, 1995).

MATERIALS AND METHODS

K(Ca) Channels Recorded in Planar Bilayers

Planar bilayers were formed on a hole (200-μm diam) in a polystyrene cup by spreading a lipid solution (25 mg/ml lipids in decane) with a small glass rod. The lipid composition was a 4:1 mixture of bovine brain phosphatidylethanolamine/1,2-diphytanoylphosphatidylcholine (Avanti Polar Lipids, Inc., Alabaster, AL). Maxi K(Ca) channels from plasma membrane vesicles of rat skeletal muscle were incorporated into planar bilayers as previously described (Lucchesi and Moczydlowski, 1991). The solution on both sides of the chamber contained 50 mM KCl and 10 mM Mops-KOH, pH 7.4. The *cis* chamber to which rat membranes were added also contained 100–200 μM $CaCl_2$ for recording at positive voltage (*trans* side corresponds to extracellular ground), and up to 0.7 mM $CaCl_2$ at negative voltage (to maintain a high open-state probability). In required experiments, 6.4 μM BPTI and 0.8–1.6 μM $BaCl_2$ were also added to the *cis* chamber. $BaCl_2$ was used to produce long channel blocks that clearly define the zero current level. The *trans* chamber also contained 0.1 mM EDTA to ensure the desired channel orientation. Bilayer recordings were made at room temperature (19–23°C) using a List-Medical Systems EPC7 patch-clamp amplifier and were stored on video tape via an Instrutech VR-10 digital data recorder. The

patch-clamp headstage was connected to the bilayer chamber via Ag/AgCl electrodes and agar-KCl bridges. The data were filtered for analysis with either an eight-pole low pass Bessel filter (902LPF; Frequency Devices Inc., Haverhill, MA), or a digital Gaussian filter (program courtesy of Dr. F. J. Sigworth, Yale University, New Haven, CT). Data were always sampled at 5–10 times the filter corner frequency (corresponding to −3 dB).

K(Ca) Channels Recorded in Patch Pipettes

Bovine aortic smooth muscle cells, a generous gift of Dr. Owen McManus (Merck Research Laboratories, Rahway, NJ), were cultured at 37°C in low glucose DME supplemented with 15% defined FBS, 25 mM Hepes, 0.1 mg/ml hydroxy-D-proline, 8.8 mM L-glutamine and 110 mg/liter sodium pyruvate. Ca^{2+}-activated K^+ channels were recorded from excised inside-out patches at room temperature (19–23°C) using an Axopatch 1-D amplifier (Axon Instruments Inc., Foster City, CA) and a Racal Store 4 FM recorder at an effective bandwidth of 10.5 kHz (measured as the −3-db bandwidth of recording system). Sylgard-coated patch pipettes (pulled from Kimax-51 glass capillaries, 2-20 MΩ tip resistance) contained 100 mM KCl, 50 nM apamin (to block SK channels), 2 mM $CaCl_2$, and 10 mM MOPS-KOH, pH 7.4. The bathing solution contained 40 μM $CaCl_2$, 100–143 mM KCl, 10 mM MOPS-KOH, pH 7.4, and either 5 μM BPTI or ~10 μM DTX.

Ultrapure KCl, $CaCl_2$ and $BaCl_2$ for bilayer solutions were obtained from Alfa Products (Ward Hill, MA). BPTI, hydroxy-D-proline and MOPS buffer were obtained from Sigma Chemical Co. (St. Louis, MO). FBS was from Hyclone Laboratories (Logan, UT) while all other tissue culture reagents were obtained from GIBCO BRL (Gaithersburg, MD). Lyophilized venom from the black mamba snake, *Dendroaspis polylepis*, was purchased from LATOXAN (Rosans, France). Pure DTX (Toxin I) was a generous gift of Prof. Alan Harvey (University of Strathclyde, Glasgow, UK).

Data Analysis

Programs for β-function fitting, rate-amplitude analysis, and single-channel simulations were written to utilize the Modula-2 based programming environment, PowerMod (HEKA-Instrutech, Great Neck, NY). Dr. F. J. Sigworth kindly provided additional programs for dwell time analysis. All programs were run on an Apple MacIntosh Quadra 650 computer.

For β-function analysis, bilayer data were filtered at 350 Hz with a digital Gaussian filter and sampled at 2.5 kHz; patch data were filtered at 5 kHz with an eight-pole Bessel filter and sampled at 25 kHz. Note that the response of an eight-pole Bessel filter approximates that of a Gaussian filter (Colquhoun and Sigworth, 1983). The application of β-function fitting to analysis of excess noise associated with BPTI- and DTX-induced substates depends upon the careful exclusion of normal channel gating activity from amplitude histograms of the substate data. In the case of maxi K(Ca) channels, this can be achieved at a particular voltage by adjusting the internal Ca^{2+} concentration to obtain a high probabilty of channel opening ($P_{open} \simeq 1$) and by carefully excluding any resolved transitions to the closed state from segments of pooled substate data (Yellen, 1984). Selection of substate data for analysis also involved checking for the absence of drift in adjacent sections of closed/Ba^{2+}-blocked states. Zeroing of the data was performed by setting the mean value of such closed/blocked states to zero. Broadening of the histogram due to background noise was compensated for by convolving the β-function with a histogram compiled from the closed-state data (Yellen, 1984). Convolutions were performed in the time domain using a numerical approximation to the convolution integral (Bracewell, 1965). Best fits of the data to the noise-broadened β-function were obtained using a Simplex algorithm (Caceci and Cacheris, 1984) and maximum likelihood criterion for goodness-of-fit (Colquhoun and Sigworth, 1983).

Initial seed values for the fits were calculated from the theoretical mean and variance relationships of a β-distribution. The probability density function, $f(y)$, of a β-distribution is given by:

$$f(y) = \frac{y^{(a-1)}(1-y)^{(b-1)}}{\int_0^1 y^{(a-1)}(1-y)^{(b-1)}\,dy}. \quad (1)$$

The mean, μ, and variance σ^2 of a β-distribution are related to the variables a and b by (Freund, 1971):

$$\mu = \left(\frac{a}{a+b}\right) \quad (2)$$

$$\sigma^2 = \mu\left(\frac{a+1}{a+b+1}\right) - \mu^2. \quad (3)$$

Simultaneous solution of Eqs. 3 and 4 for the two unknowns, a and b, yields:

$$a = \mu\left[\frac{\mu(1-\mu)}{\sigma^2} - 1\right] \quad (4)$$

$$b = (1-\mu)\left[\frac{\mu(1-\mu)}{\sigma^2} - 1\right]. \quad (5)$$

In the case of a reversible, two-state process with transition rates, α and β, the variables, a and b in Eqs. 1–5, are related to the transition rates by the relations: $a = \alpha\tau$, $b = \beta\tau$, where τ is the time constant of a single-pole filter (Yellen, 1984). An empirical relation between the −3-dB cutoff frequency of an eight-pole Bessel filter, f, with that of a single-pole filter, f_0, is: $f_0 = 0.7f$ and $\tau = 0.228/f$ (Yellen, 1984). The theoretical mean and variance of the β-distribution can be related to the mean and variance of the actual current record by normalizing to the single-channel current and subtracting background (baseline) variance. Values of α and β calculated from Eqs. 4 and 5 were always close to the final values obtained by maximum likelihood fitting, typically within ~5%.

The rate-amplitude (dI/dt vs I) analysis method of Tyerman et al. (1992) was used to identify nodes of stable current level in high-resolution records of BPTI-substates. For this analysis, dI/dt was computed as the linear-regression slope of a running three-point window of data. The absolute value of this slope was plotted as a function of mean current as in Root and MacKinnon (1994).

Half-amplitude threshold-crossing analysis was used to measure channel dwell times. Dwell time histograms were compiled and fitted as described by Sigworth and Sine (1987). Correction of the observed time constants for missed events was performed by the method of Colquhoun and Sigworth (1983) for the case of a two-state process. Current amplitude levels were variously measured from the peaks of amplitude histograms, by cursor alignment through filtered current levels, or by calculating mean current of resolved openings using long closures or Ba^{2+}-blocking events to define the zero current level.

Nonlinear fitting of I-V relations to a Boltzmann transform and fitting of rate constants to exponential functions of voltage were performed with the curve fitting utility of Sigmaplot software (Jandel

Scientific, Corte Madera, CA). Fitting the *I-V* curve of the BPTI-substate to a three-barrier, two-site Eyring energy profile was performed with the use of the AJUSTE program (Alvarez et al., 1992).

Monte Carlo Simulation of the Effect of Fast, Filtered Fluctuations on Unitary Current Levels Measured by Amplitude Histograms

The purpose of this simulation was to evaluate the magnitude and types of errors that arise when amplitude histograms are used to measure the amplitude of filtered unitary channel currents in the presence of excess open-state noise. A pseudo-random number generator (Press et al., 1986) was used to simulate single-channel records for a linear, Markovian kinetic scheme of C(closed)-O(open)-S(substate). This scheme includes four rate constants j, k, α, and β (defined in Fig. 11), two for each reversible transition between the three states. The magnitude of all rate constants is defined relative to the filter corner frequency, f, and is therefore unitless. The C, O, and S states were defined to have a relative current amplitude of 0, 1, and 0.25, respectively. In this scheme, excess noise is generated by the reversible transition between the open state (O) and the substate (S). The rate constants for the C-O transition (k, j) were fixed at a slow, resolvable magnitude (k = f/83, j = f/50) to conveniently provide some resolved events in the C level. Both of the rate constants for the O-S transition (α, β) were systematically varied over four log units relative to the filter frequency from 0.1 f to 100 f in steps of 0.1 log units. This range is adequate for our purpose since limiting behavior is found at the extreme values. The program analyzes the simulated single-channel record to determine the apparent open-state current level with the use of an all-points amplitude histogram. The criteria that the program uses to find the open-state current level are designed to mimic the practical approach that a human operator would use based on methods currently described in the channel literature.

The program works by initially writing noiseless data for a given set of rate constants to an array of 600,000 points. In this array an open, closed, or substate dwell time is represented by a string of successive points all having the same value (since the current level is constant in any given dwell time). The dwell times are digitized at a sampling rate of 200 times the filter frequency, f. This means that the fastest simulated rates (100 times the filter frequency) correspond to an average dwell time that is represented by a string of two data points in the array. Dwells that are shorter than one array point are written as a fraction of the open channel current. This leads to a type of very light filtering for the fastest events simulated that is negligible compared to the Gaussian filtering that follows. The simulation procedure was designed to avoid any significant sampling artifacts over the whole range of explored rate constants.

The simulated, noiseless data are next filtered with a digital Gaussian filter (Colquhoun and Sigworth, 1983), and compressed 20-fold. The resulting record is equivalent to a single-channel record digitized at 10 times the filter frequency. Finally, simulated background noise with a Gaussian amplitude distribution and a standard deviation set at 5% of the open-channel level (σ = 0.05) is added to the record. When the simulated record has been created, an all-points amplitude histogram is compiled by sorting the data points into bins of equal width. The bin width was 1/50 of the open to closed current amplitude.

To measure the apparent open-state amplitude from the simulated record, the program first decides whether dwell times in the O(open) state are cleanly resolved based on the criterion: $f \geq \alpha$, where α is the rate constant for the O→S transition. If the open state is resolved, the program identifies the highest frequency bin of largest conductance as an estimate of open-channel current. If open-state dwell times are not resolved, the program decides whether dwell times in the S(substate) are resolved based on the criterion: $f \geq \beta$, where β is the rate constant for the S→O transition. If substate dwell times are resolved, the program fits a half-Gaussian curve (σ = 0.05) to the tail of the amplitude histogram. This procedure emulates the tail-fit method of Wonderlin and French (1991), which is analogous to placing a horizontal cursor near the tips of the highest amplitude opening events (e.g., Fig. 13, second and third records from the top). The peak of this Gaussian curve is taken as an estimate of the open-channel current. This "fit" is actually an alignment performed by minimizing the quantity ([4 × chi-squared] − [log-likelihood]). This criterion was a practical choice since neither standard log-likelihood nor chi-squared minimization alone provided a good fit in all situations. (This is not surprising since the tail of the amplitude distribution is non-Gaussian.) If neither the open-state nor the substate dwell times are resolved, and the α, β rate constants are in the applicable range for a β-function (i.e., α and $\beta \geq$ 8.772f [Yellen, 1984]), then the program again identifies the highest conductance peak as an estimate of open channel current. Finally, if neither the open state nor the substate dwell times are resolved, and the α, β rate constants are not in the proper range for a β-function, then the program again fits a half-Gaussian function to the tail of the amplitude histogram. Some practical restrictions were also added to the fit; e.g., the program was not allowed to choose a bin with <10 events as the open state. Clearly, like its human counterpart, the decision process that the program uses to measure unitary current levels is imperfect; however, it effectively simulates the outcome of using amplitude histograms and cursor alignment techniques to measure single-channel currents in the presence of excess noise arising from an unresolved two-state process.

To calculate the variance (in Fig. 12 *C*) expected for a filtered, two-state switching process between two levels (i = 0 and i = 1), where $\sigma^2_{\text{unfiltered}} = \alpha\beta/(\alpha + \beta)^2$, we used the following relation for a Gaussian filter as derived by Ogden and Colquhoun (1985):

$$\frac{\sigma^2_{unfiltered}}{\sigma^2_{filtered}} = \frac{\exp(-z^2)}{[1 - erf(z)]} . \tag{6}$$

In Eq. 6, $z = (\ln 2)^{0.5}(f_c/f)$, f_c is the corner frequency of the unfiltered Lorentzian spectrum ($f_c = \{\alpha + \beta\}/2\pi$), and f is the corner frequency of the filter. The following approximation can be used to evaluate the error function, $erf(z)$, as described (Colquhoun and Sigworth, 1983):

$$erf(z) = 1 - (a_1 t + a_2 t^2 + a_3 t^3) \exp(-z^2) . \tag{7}$$

Where $t = 1/(1+pz)$ and $p = 0.47047$, $a_1 = 0.3480242$, $a_2 = -0.0958798$, $a_3 = 0.7478556$. Substituting this expression into Eq. 6 gives:

$$\sigma^2_{filtered} = \sigma^2_{unfiltered}(a_1 t + a_2 t^2 + a_3 t^3) \tag{8}$$

RESULTS

Excess Noise Associated with BPTI-induced Substates Is Well Described by a β Distribution

This study was originally motivated by the effect of dendrotoxin and mamba snake venom on the internal (intracellular) side of maxi K(Ca) channels incorporated into planar bilayers. As illustrated in Fig. 1 *A*, venom from the black mamba snake, *D. polylepis*, induces long-lived periods of lower apparent unitary conductance in a single K(Ca) channel. This widely studied channel normally exhibits gating transitions between two major current levels, closed (or shut) and open. Previous work by Lucchesi and Moczydlowski (1990) showed that the pure dendrotoxin homologue, Toxin I (DTX), reversibly induces discrete subconductance events at ~70% of the open current level. Thus, the 70% sublevel induced by the crude venom (Fig. 1 *A*) most likely represents periods when DTX is bound to the channel. (Our preliminary studies suggest that the less frequent sublevel at ~50% of open-channel current in Fig. 1 *A* is probably due to a different DTX homologue in the venom mixture.) The records of Fig. 1 *A* are displayed at a level of filtering (50 Hz) that is typically used to characterize long-lived (>1 s) toxin-channel interactions. This figure also illustrates two important features of this interaction: (*a*) Ca^{2+}- and voltage-dependent channel gating, which corresponds to the rapid flickering seen in Fig. 1 *A*, is not strongly affected by binding and unbinding of DTX (Lucchesi and Moczydlowski, 1990). (*b*) At low resolution (~50 Hz), DTX-induced substates visually appear as "clean" reductions in channel amplitude, with a similar amount of excess noise at the sublevel compared to the control, open-channel level. (In this paper, the term, excess noise, is defined as noise greater than expected from the shot noise due to ion transport and background noise as evaluated from well-resolved closed states of the channel; e.g., middle of top trace in Fig. 1 *A*.)

Fig. 1 *B* illustrates a second observation previously made in studies dealing with the structure-activity basis of the DTX-channel interaction (Lucchesi and Moczydlowski, 1991). The homologous protein, BPTI, induces discrete substates of shorter duration than those of DTX, but with more pronounced *I-V* rectification. While the control traces of Fig. 1 *B* at +30 and at −30 mV demonstrate the characteristic ohmic *I-V* behavior of maxi K(Ca) channels, the resolved substate interruptions in the presence of BPTI exhibit a smaller current level at +30 than −30 mV. As briefly stated in the Introduction, previous work has led to the conclusion that DTX and BPTI perturb conduction of K^+ through the maxi K(Ca) channel by an allosteric mechanism that involves a conformational change of the pore region. The specific question that we address here is: what type of conformational change of the ion permeation pathway can explain the conversion of a nearly ohmic, high-conductance pore to an inwardly rectifying, low-conductance pore.

Dani and Fox (1991) previously considered this general problem in a theoretical study using Eyring barrier models of channel permeation to explore the basis of subconductance behavior. They distinguished two classes

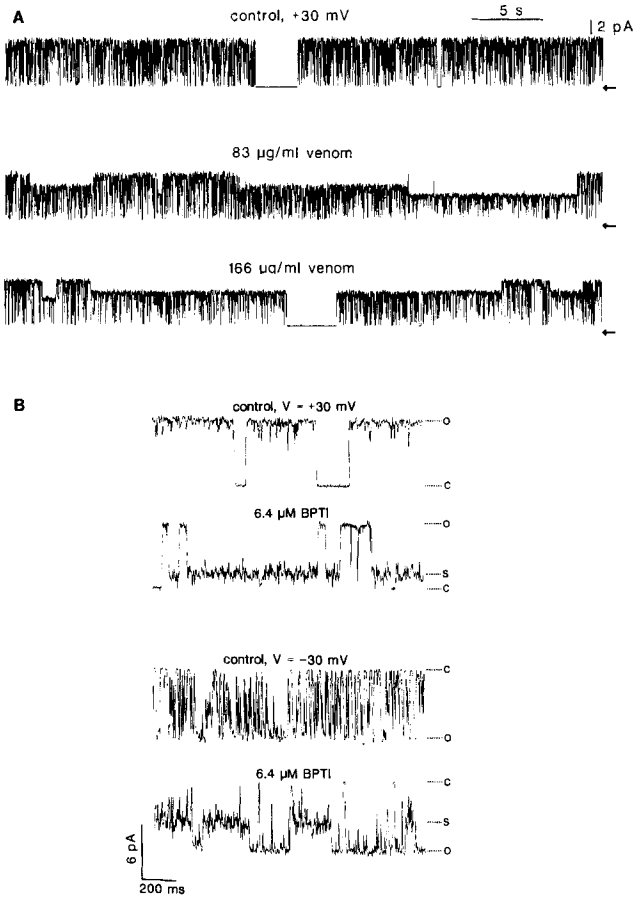

FIGURE 1. Subconductance behavior induced by venom from *D. polylepis* and BPTI in single maxi K(Ca) channels recorded in a planar bilayer. (*A*) Current records before and after addition of *D. polylepis* venom. Control conditions: 10 mM MOPS-KOH, pH 7.4, symmetrical, 100 mM KCl, and 300 μM $CaCl_2$ internal, 50 mM KCl external. The second and bottom traces are representative data recorded after addition of 83 and 166 μg/ml venom to the internal chamber, respectively. Holding voltage = +30 mV. The record was filtered at 50 Hz and sampled at 500 Hz. Arrows to the right of each trace indicate the zero current level. (*B*) Current records before and after addition of BPTI. Control conditions: 10 mM MOPS-KOH, pH 7.4, and 50 mM KCl symmetrical, 100 μM $CaCl_2$ internal, and 100 μM EDTA external. The first (V = +30 mV) and third traces (V = −30 mV) from the top were recorded under control conditions. The second and fourth traces show representative segments after addition of 6.4 μM BPTI and an additional 100 μM $CaCl_2$ to the internal side to increase P_{open}. Records are filtered at 100 Hz and sampled at 1 kHz. Markers to the right of each trace denote closed (*C*), open (*O*), and substate (*S*) current levels.

of models that involve conformational changes of the ion conduction pathway. Fig. 3 illustrates these two alternative models and shows how either model could explain the effect of BPTI.

In the first model (Fig. 2 *A*), the structure of the open channel pore is assumed to be relatively rigid. In this "rigid pore" or "static" model, the filtered mean current level of an open state or a substate reflects a well-defined pore conformation represented by a single energy profile. With this approach, the ohmic unitary *I-V* behavior of the open channel can be simulated by a symmetrical three-barrier, two-site, Eyring-type model for K^+ conduction through maxi K(Ca) channels similar to those proposed previously (Yellen, 1984; Cecchi et al., 1987; Villarroel and Eisenman, 1987; Villarroel, 1989). In such rate-theory models the maxima correspond to energy barriers for ion movement and the minima correspond to binding sites for the ion. By this formalism, the inwardly rectifying *I-V* relationship of the BPTI-induced substate can be simulated by a different three-barrier, two-site energy profile that has a higher barrier for K^+ at the intracellular side and slightly shallower energy wells. Although the energy profiles used to fit the open channel and substate *I-V* data in Fig. 2 *A* are not unique, there is basically only one way a rigid pore model can generate a rectifying *I-V* curve for symmetrical ionic conditions: an asymmetric energy profile is required. (Asymmetric surface potential or a voltage-dependent fast block can also give rise to apparent rectification. These mechanisms are ruled out here by the lack of dependence of the relative substate level on ionic strength, the concentration of BPTI, and the concentration of possible blocking ions such as Ca^{2+} and H^+ [Lucchesi and Moczydlowski, 1991; Moss and Moczydlowski, unpublished results].)

In the second "fluctuating barrier" model of Fig. 2 *B*, the dynamic nature of protein structure is emphasized. It is assumed that a unitary current level represents an average of pore conformations that, individually, may differ substantially in their conductance. In the simplest situation, a conductance level might arise from rapid, unresolved switching between conducting and nonconducting states due to fluctuations of the channel structure. Filtering, which unavoidably accompanies any single-channel measurement, produces a time-average of the channel current and may thus disguise a rapidly fluctuating channel as a stable, intermediate subconductance level. In contrast to the rigid pore model, a rectifying *I-V* curve can arise from symmetrical energy profiles for permeation if rate constants for the

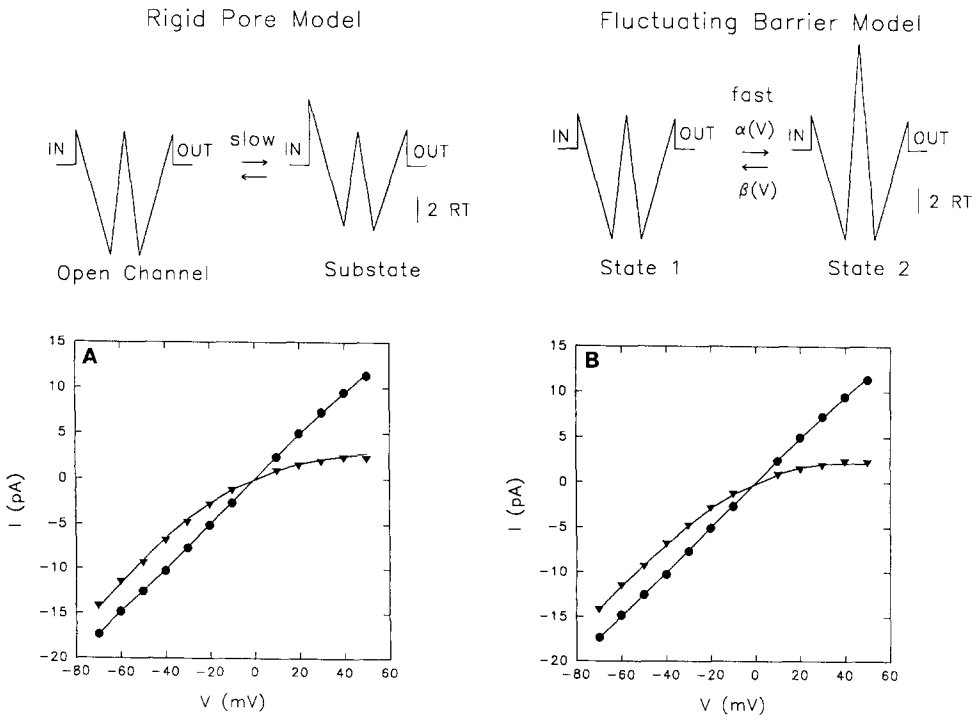

FIGURE 2. Two alternative energy barrier models for BPTI-induced substates. (*A*) Rigid pore model with the open state and the subconductance state represented by two distinct energy profiles. Unitary *I-V* data for the open channel (●) and the rectifying BPTI substate (▼) are fit (*solid lines*) by the respective three-barrier, two-site energy profiles shown above. Ion-binding sites (wells) are placed at 35% and 65% of the way through the transmembrane electric field and energy barriers are at 0, 50, and 100%. The open-channel energy profile for K^+ permeation is based on that proposed by Villarroel and Eisenman (1989) and Villarroel (1989). (*B*) Fluctuating barrier model. Open-channel data (●) is the same as in *A* fit using the energy profile of State 1. Subconductance events are assumed to represent the filtered average of unresolved transitions between a normal open state (*State 1*) and a very low conductance state (*State 2*). Substate data were fit to: $I_{substate} = I_{open}\, K(V)/\{K(V) + 1\}$, with $K(V) = K(0)\exp(-z'FV/RT)$, where $K(V)$ and $K(0)$ are the ratio of transition rates β/α, at voltages, V, and $V = 0$, respectively. In this notation, z' is the gating charge associated with the fluctuation process, F is Faraday's constant, R is the gas constant and T is absolute temperature. The solid line fit to the substate data (▼) uses $z' = 0.64 \pm 0.01$ and $K(0) = 0.79 \pm 0.02$. Data were obtained under the following conditions: 50 mM KCl, 10 mM MOPS-KOH, pH 7.4, symmetrical, 200 μM $CaCl_2$, and 1 μM BPTI internal, 0.1 mM EDTA external. Standard errors are smaller than the symbols.

rapid fluctuation are voltage dependent. We arbitrarily chose two symmetric energy profiles in Fig. 2 *B* to emphasize that major differences in interpretation are possible for static vs dynamic models. As illustrated in Fig. 2 *B*, a fluctuating barrier model of the BPTI-induced substate might involve a fast, voltage-dependent equilibrium between the normal open-channel conformation (State 1) and a nearly closed conformation (State 2) with a high internal barrier that is assumed to conduct at a negligible rate. In this case, a voltage-dependent equilibrium constant for the two states may be described by a Boltzmann function:

$$K(V) = \frac{P_{\text{State1}}}{P_{\text{State2}}} = K(0) \exp(-z'FV/RT) \qquad (9)$$

where the ratio of equilibrium probabilities (P) in each state is equal to the product of the equilibrium constant at 0 mV, $K(0)$ and an exponential function of voltage, V; a gating charge, z'; absolute temperature, T; and, the physical constants, F and R. In Fig. 2 *B*, the open-state *I-V* curve is simulated by the same energy profile used in Fig. 2 *A*, but the *I-V* curve for the BPTI-induced substate is fit by an appropriate transformation of Eq. 9 with best-fit parameters, $z' = 0.64 \pm 0.01$ and $K(0) = 0.79 \pm 0.02$. According to this model, the open-current level of the channel would represent a static pore or an equilibrium process greatly shifted toward State 1. The substate current may be interpreted as a large shift of the conformational equilibrium toward State 2. The voltage dependence of the two-state equilibrium as inferred by z' is equivalent to that of a monovalent charge moving 64% of the way through the electric field. In this interpretation, the strong inward rectification induced by binding of BPTI reflects the destabilization of a relatively rigid open-channel structure to expose a fast, voltage-dependent equilibrium between two different conformations of the channel-BPTI complex. The model of Fig. 2 *B* is actually a special case of the general fluctuating barrier model originally proposed by Läuger et al. (1980). Specifically, the rate constants of the conformational process (α, β) are assumed to be much faster than the filter frequency, State 2 is assumed to be nonconducting, and the ion translocation rates are assumed to be much faster than α and β so that K^+ is in rapid equilibrium with State 1 and State 2. This particular case was previously discussed by Läuger (1983) with respect to single-channel rectification. The equations that we have used to fit the substate *I-V* curve (Fig. 2 *B*, legend) are equivalent to Eqs. 25 and 28 in this latter reference.

In principle, these two conformational models for the BPTI-induced substate can be experimentally discriminated by the noise characteristics of the substate current. A rigid-pore model predicts that current noise associated with the substate level will be low, reflecting only the background noise of the recording system plus low intensity shot noise of ion movement (Heinemann and Sigworth, 1993). In contrast, a fluctuating barrier model predicts excess noise due to the fast conformational changes that modulate the permeation process. Inspection of the top two records in Fig. 1 *B* filtered at 100 Hz suggests that current noise at the open-channel level and the BPTI-substate level is somewhat greater than the noise of the two well-resolved closed states in the control (*top*) record. Since the closed state is assumed to reflect background recording noise, fast channel fluctuations may contribute excess noise to the substate and the open state. The observation that BPTI-induced substates tend to be excessively noisy, led us to improve recording conditions by using smaller, lower-noise bilayers and a better amplifier to enable us to analyze this aspect of the data.

In practical terms, single-channel recording is limited by the necessity to filter high-frequency background noise that is especially serious for planar bilayers with large surface area (Wonderlin et al., 1990*a*). Comparison of Fig. 1 *B* (filtered at 100 Hz) with Fig. 3 (filtered at 500 Hz) illustrates the effect of filtering. At 500 Hz, the magnitude of noise associated with each current level is increased. However, the magnitude of noise observed for closed and open states in Fig. 3 is roughly similar. In contrast, the noise exhibited by the inwardly rectifying BPTI-substate is dramatically larger at 500 Hz, suggestive of a process like that proposed in Fig. 2 *B*. For the particular model of Fig. 2 *B*, in which the channel rapidly switches between two amplitude levels, the probability density of the filtered signal is theoretically described by a β-distribution under particular filtering conditions (FitzHugh, 1983; Yellen, 1984).

Plots of frequency (N) vs current amplitude bins (to the right of each trace in Fig. 3) show that amplitude histograms of substate data compiled at four different voltages are indeed well described by β-functions. Each of the substate amplitude histograms is considerably broader than the histogram of Gaussian baseline noise compiled from the zero-current level (Fig. 3, −50 mV). The continuous β-function used to fit each of the substate amplitude histograms assumes that in the apparent substate, the channel is rapidly switching between the fully closed and fully open-current levels of the normal control channel. As outlined by Yellen (1984), this analysis can be used to derive the underlying transition rates for a two-state process because α and β, along with the filter frequency, determine the width and skew of the amplitude histogram (FitzHugh, 1983; Yellen, 1984). Rate constants (α and β) derived from fits of amplitude histograms are plotted in Fig. 4 *A* as a function of voltage. This plot shows that both α and β are well described by exponential functions of voltage in

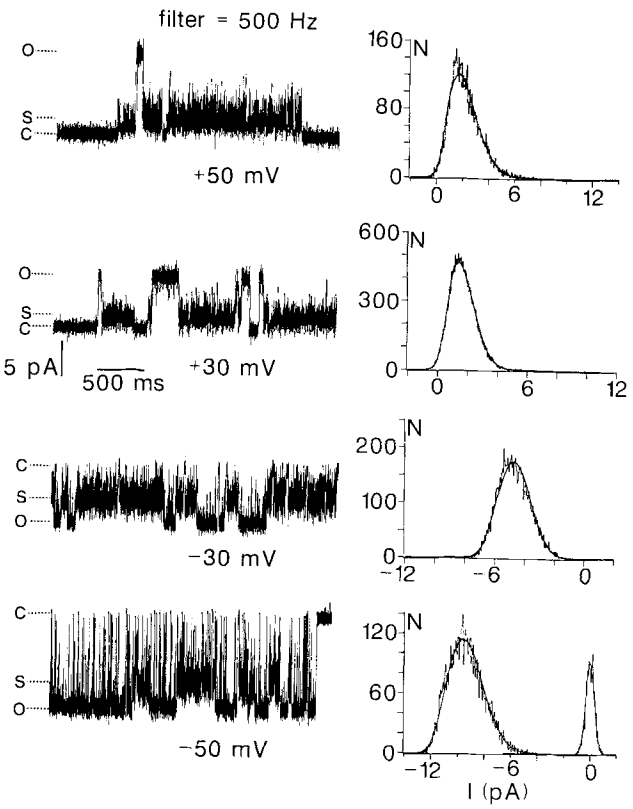

FIGURE 3. Amplitude histograms of excess current noise associated with BPTI-induced substates are well described by a β-distribution. BPTI-induced substates were recorded in a single maxi K(Ca) channel in a planar bilayer as described in Fig. 2. The four traces at the left show representative data segments at +50, +30, −30, and −50 mV filtered at 500 Hz. Excess noise associated with the substate is demonstrated by broad amplitude histograms of separately compiled substate segments in comparison to the narrow distribution compiled from the closed state. The closed-state histogram is shown as a peak centered at 0 pA for the −50 mV record and is fit with a Gaussian function (*solid curve*). Amplitude histograms of substate data are superimposed by maximum-likelihood fits (*solid curve*) to a β-distribution. Rate constants derived from these fits are plotted in Fig. 4 *A*.

the range of −50 to +50 mV, with α increasing and β decreasing with positive voltage. This result is expected from transition-state theory for the model of Fig. 2 *B* according to the following equation:

$$K(V) = \frac{\beta(0)\exp(-z'_{\beta}FV/RT)}{\alpha(0)\exp(z'_{\alpha}FV/RT)}. \qquad (10)$$

Best-fit parameters (zero-voltage rate constants, α(0) and β(0), and relative gating charges of the transition state, z'_{α} and z'_{β}) derived from fitting these rate constants to exponential functions of voltage are given in the legend of Fig. 4. Comparison of these parameters with those derived from equilibrium analysis of the substate *I-V* curve in Fig. 2 *B* according to Eq. 9 shows reasonable agreement between the equilibrium and kinetic approach: $K(0) = \beta(0)/\alpha(0)$, (0.79 ± 0.02 vs 0.62 ± 0.05, respectively) and $z' = z'_{\alpha} + z'_{\beta}$ (0.64 ± 0.01 vs 0.76 ± 0.08, respectively). This agreement is further illustrated by the comparison in Fig. 4 *B* of the directly measured mean current values with predictions computed from rate constants derived from β-function analysis.

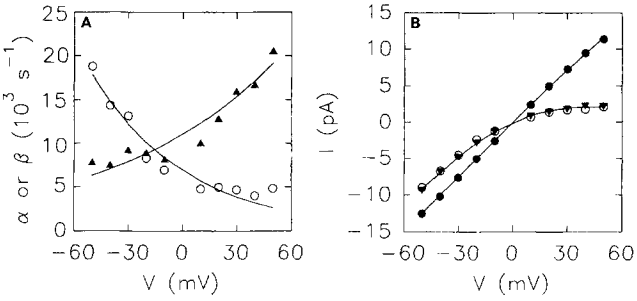

FIGURE 4. Voltage dependence of transition rates underlying BPTI-induced substates. (*A*) Amplitude histograms of BPTI-substates were fit by a β-function (as in Fig. 3) to obtain α (▲) and β (○) at various voltages. Solid curves correspond to the functions: $\alpha(V) = \alpha(0)\exp(z'_{\alpha}FV/RT)$ and $\beta(V) = \beta(0)\exp(-z'_{\beta}FV/RT)$, using $z'_{\alpha} = 0.28 \pm 0.03$, $z'_{\beta} = 0.48 \pm 0.05$, $\alpha(0) = 11{,}000 \pm 500\ s^{-1}$ and $\beta(0) = 6{,}870 \pm 530\ s^{-1}$. (*B*) Substate *I-V* curve predicted from noise analysis. Directly measured mean current values for the BPTI-induced substate (▼) are compared to predictions from a β‴-function analysis (○) calculated according to: $I_{substate} = I_{open}\,\beta(V)/[\beta(V) + \alpha(V)]$. The open state *I-V* curve (●) from Fig. 2 is shown for comparison.

Analysis of Subconductance Events Induced by BPTI and DTX in Single K(Ca) Channels Recorded at High Resolution in Patch Pipettes

The preceding β-function analysis predicts that the noisy BPTI-induced substate is actually composed of brief openings with a dwell time of ~90 μs and brief closures with a dwell time of ~145 μs at 0 mV. Channel dwell times in this range are not resolvable at the filtering level needed for our planar bilayer recording system (<1 kHz), but are within the resolution limit of low-noise patch recording. To verify this interpretation of the substate process, we recorded single K(Ca) channels from bovine aortic smooth muscle cells using the excised patch technique to examine the effect of BPTI at higher resolution. Fig. 5 shows a direct comparison of BPTI-induced substate activity for a single K(Ca) channel recorded in a planar bilayer (*top*) and an inside-out patch (*bottom*) with both records filtered at 100 Hz. Qualitatively similar behavior is observed for the two types of recordings, but there are several quantitative differences. As seen in Fig. 5, BPTI-induced substate periods of activity recorded in patch pipettes have a longer average duration than those observed in the bilayer recordings. At +20 mV, the mean dwell time of the exponentially distributed substate durations and

their standard deviation (SD) measured in patches was 5.6 ± 7.4 s (± SD, n = 46) vs 0.54 ± 0.68 s (± SD, n = 121) in the bilayer. Also, the mean current level of BPTI-induced substates in the patch was lower and rectified more strongly than that measured in bilayers (compare *I-V* data of Figs. 4 *B* and 8 *F*). When compared at 100 Hz filtering, patch recordings also exhibited distinctive closing transitions within the substate periods that are not observed in the bilayer records (Fig. 5). The exact basis for these quantitative differences in the BPTI-induced substate phenomenon for bilayer vs patch is presently unknown. It is possible that a difference in membrane environment (reconstituted vs native) or a different tissue source of the channels (smooth muscle vs skeletal muscle) may explain this discrepancy. Nevertheless, in both systems it appears that BPTI causes discrete interruptions in the single-channel current without completely blocking the channel.

Fig. 6 illustrates the effect of filtering on BPTI-induced substates as recorded in a patch pipette. The top trace in Fig. 6 *A* (+40 mV, opening is upward) first shows a patch recording filtered at 0.5 kHz, as in the planar bilayer experiment of Fig. 3. At this resolution, the BPTI-induced events appear as noisy, low-conductance substates periodically interrupting normal channel openings. When the filter bandwidth of this record is increased to 10.5 kHz (Fig. 6 *A*, second trace from top), the intervals that resemble "substates" at 0.5 kHz, now appear as intervals of low open-state probability that are composed of many brief opening events. Further expansion of the time base reveals, that even at 10.5 kHz, many of the individual opening events underlying the substate are not fully resolved (Fig. 6 *A*, third and fourth traces from top). Fig. 6 *B* shows a similar resolution of a BPTI-induced substate interval at negative voltage (−40 mV, opening is downward). Comparison of the records at +40 mV (Fig. 6 *A*) and −40 mV (Fig. 6 *B*) shows that the flickering process underlying the substate is voltage dependent in the manner expected from the noise analysis of Fig. 4 (i.e., openings are

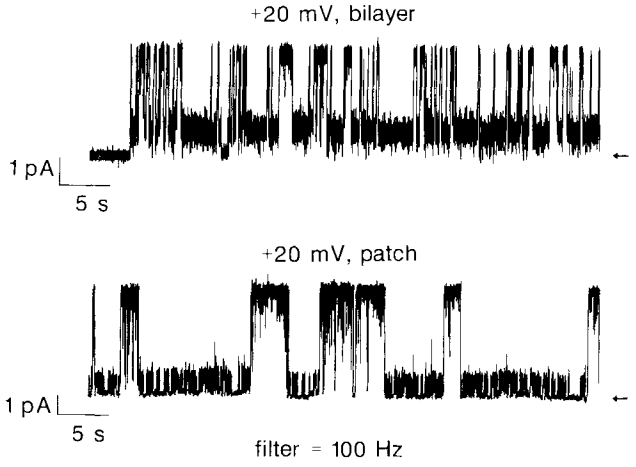

FIGURE 5. Comparison of BPTI-induced substates for a rat skeletal muscle K(Ca) channel recorded in a planar bilayer (*upper trace*) with that of a bovine smooth muscle K(Ca) channel recorded in a patch pipette (*bottom trace*). The zero-current level is indicated by an arrow at the right. The mean dwell time of BPTI-induced substates was measured as 0.54 ± 0.68 s (± SD, n = 121) in the bilayer and 5.6 ± 7.4 s (± SD, n = 46) in the patch. Recording conditions were 50 mM (*bilayer*) or 100 mM (*patch*) symmetrical KCl and 500 μM (*bilayer*) or 40 μM (*patch*) internal $CaCl_2$. V = +20 mV, 100 Hz filtering.

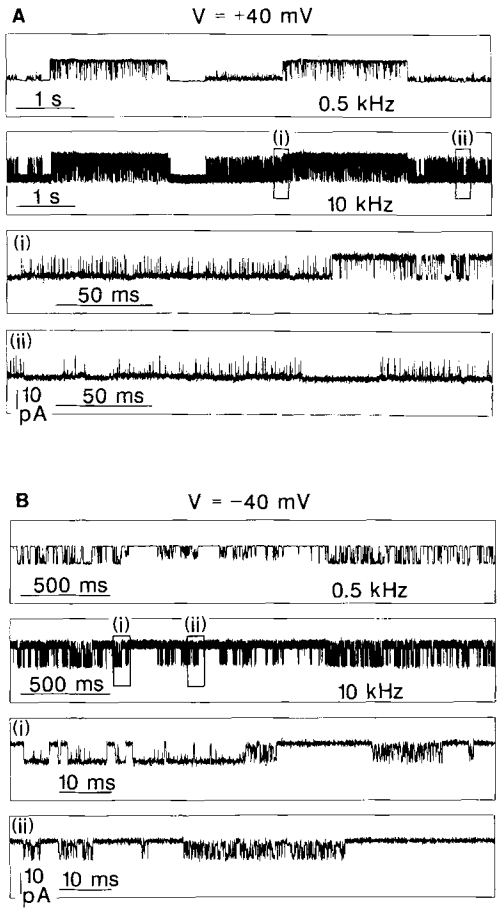

FIGURE 6. High resolution patch recordings of BPTI-induced substates in a maxi K(Ca) channel from a bovine aortic smooth muscle cell. (*A*) The top trace shows data from a single K(Ca) channel held at +40 mV and filtered at 500 Hz (digital Gaussian filter). Two long bursts of normal channel openings (open is upward) are interrupted by noisy substate activity. The second trace from the top shows the same data filtered at 10.5 kHz (−3 db bandwidth of recording system) illustrating that noisy substate periods result from many brief transitions to the open state. The third and fourth traces show time-expanded views of boxed segments labeled *i* and *ii*, respectively, in the second trace. (*B*) Similar increase in filter bandwidth and time base for the same channel in *A* held at −40 mV. The top trace filtered at 500 Hz shows two bursts of normal channel opening events (open is downward) interrupted by a period of substate activity and complete channel closures observed in the center of the record.

shorter and closings are longer at positive voltage). This voltage dependence is in the opposite direction to that underlying the normal Ca^{2+}-dependent gating of this channel, which increases open probability at increasingly positive voltage, and represents a clear distinction between these two processes.

Careful inspection of the "closed" level within the substate interval resolved at 10.5 kHz suggests that the channel is not quite fully closed, as indicated by bursts of brief openings that appear to arise from a low conductance pedestal (Fig. 6 *A*, *bottom trace*). This point is demonstrated more clearly by the amplified records and analysis of Fig. 7. The top trace in Fig. 7 *A* shows an expanded segment of single-channel data taken at +40 mV and filtered at 10.5 kHz (opening is upward). The middle portion of the record represents a true closed state (zero current level) of the channel as identified by long periods of no channel activity at other places in the recording. The bursts of brief opening events on either side of this closure represent high-resolution recordings of BPTI-substate activity. The mean current level of "closures" within this substate burst appears to be slightly higher than the zero current level. Tyermann et al. (1992) introduced a method for identifying discrete conductance levels by plotting a running average of $|dI/dt|$ vs mean current (rate-amplitude plot). In such a plot resolved conductance levels appear as nodes, or clusters of points, centered on the resolved current level. For example, closed-state data from the central portion of the trace shown in Fig. 7 *A* was used to construct the $|dI/dt|$ plot in Fig. 7 *B*. As expected for a single, nonconducting state, there is only one node of activity clustered around the zero current level. This can be compared to the plot in Fig. 7 *C* constructed from the bursts of activity within the BPTI-induced substate (left and right sides of the trace Fig. 7 *A*). In this plot, a strong node of activity is resolved, but the data points are clustered around a nonzero value of ~1 pA. This node at ~1 pA represents the current pedestal from which bursts of openings occur. A second node of activity corresponding to a current level for the open state conductance is not seen because channel openings are too brief to be resolved; however, the trajectory of $|dI/dt|$ points indicate that openings rise to a level near 9 pA. The nonzero current pedestal at +40 mV can also be demonstrated by the more traditional method of an all-points amplitude histogram, as shown by the inset to Fig. 7 *B*.

Similar behavior of the highly resolved substate activity is observed at negative voltage (−40 mV), as illustrated by the record of Fig. 7 *D* (opening is upward). A $|dI/dt|$ plot compiled from the zero-current level (Fig. 7 *E*) is compared to that constructed from the rapidly flickering activity resolved for the BPTI-substate filtered at 10.5 kHz (Fig. 7 *F*). The control $|dI/dt|$ plot for the

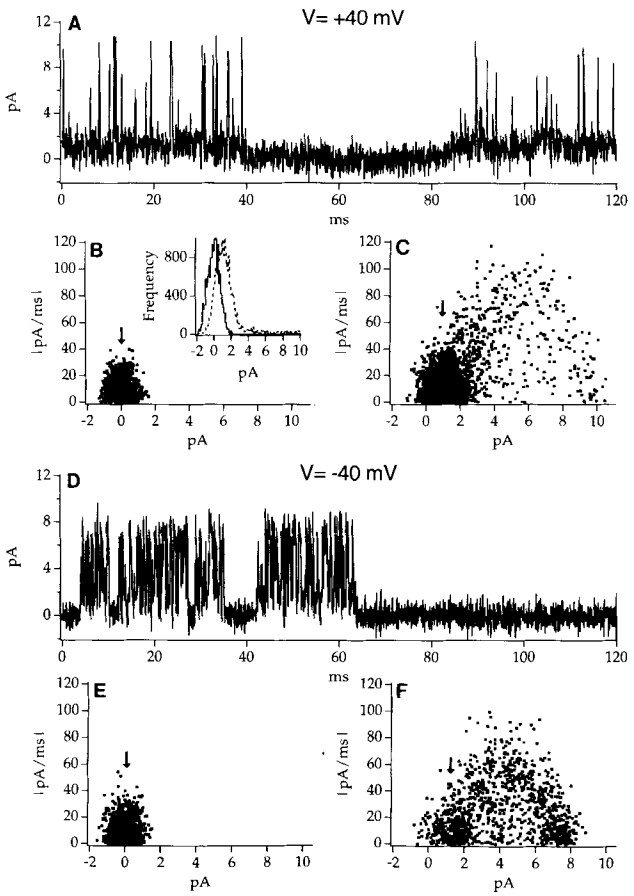

FIGURE 7. Bursts of brief openings within a BPTI-induced substate originate from a low-conductance pedestal. (*A*) Expanded view of brief openings during a BPTI-induced substate as resolved at +40 mV and 10.5 kHz filtering. Two bursts of very brief openings lie on either side of a complete closure in the center of the record. The current level of closed dwell times that occur between brief openings is significantly higher than the zero current level. (*B*) A plot of $|dI/dt|$ vs current amplitude for the central (zero current) portion of trace *A*. As noted by the arrow, a node of $|dI/dt|$ values is centered around the zero current level. The solid line in the inset corresponds to an all-points amplitude histogram separately compiled from the closed state in the midsection of trace A. The shifted dotted line in the inset with a peak at ~1.2 pA corresponds to an amplitude histogram separately compiled from substate bursts in trace *A*. (*C*) A plot of $|dI/dt|$ vs current amplitude compiled from the substate period on either side of the long channel closure in the middle of trace *A*. The node marked by an arrow is centered at a value of ~1 pA. (*D*) Expanded view of rapid flickering during a BPTI-induced substate as resolved at −40 mV and 10.5 kHz filtering. Channel opening is oriented upward for ease of direct comparison with *A*. (*E*) $|dI/dt|$ plot constructed from a long closure from the right hand side of trace *D* shows a node of activity at the zero current level. (*F*) $|dI/dt|$ plot compiled only from the two bursts of activity on the left side of trace *D* shows a node centered at a nonzero value of ~1.6 pA.

complete closure shows a single node at the zero current level. In contrast, the substate burst exhibits two nonzero nodes of $|dI/dt|$. The node centered near 7.5 pA corresponds to the open current level while the node centered near ~1.6 pA corresponds to a current pedestal underlying the substate activity. The results of Figs. 6 and 7 show that apparent BPTI-induced subconductance states observed at a filter frequency in the range of 50–500 Hz are actually composed of brief events that transit between current levels that are close to the fully open and closed states of the normal channel as postulated in the fluctuating barrier model of Fig. 2 *B*. However, the demonstration of a nonzero current pedestal in Fig. 7 indicates that the apparent subconductance event has a conductance substructure that is more complex than a simple open-closed process.

We also assessed the voltage dependence of BPTI-induced current fluctuations in patch recordings for comparison with the β-function analysis of bilayer data. Since the openings and closures were fairly well resolved at 10.5 kHz, a conventional 50% threshold-crossing criterion was used to construct histograms of dwell times in the low-conductance current pedestal (closed) state (Fig. 8, *A* and *C*) and dwell times in the open state (Fig. 8, *B* and *D*). Both types of dwell time histograms were fit to a single-exponential distribution using logarithmic binning. After correcting the observed time constants for missed events, the corrected rate constants for closing and opening were plotted and fit to exponential functions of voltage according to Eq. 10 (Fig. 8 *E*). The voltage-dependence of the transition rate constants derived from patch records ($z'_\alpha = 0.30 \pm 0.07$, $z'_\beta = 0.57 \pm 0.06$) is similar to that derived from β-function analysis of the bilayer data as described above ($z'_\alpha = 0.28 \pm 0.03$, $z'_\beta = 0.48 \pm 0.05$). However, the zero-voltage closing rate was faster ($\alpha(0) = 30{,}300 \pm 3{,}300\ s^{-1}$) and the zero-voltage opening rate was slower ($\beta(0) = 3{,}690 \pm 390\ s^{-1}$) than the corresponding values measured for the bilayer data ($\alpha(0) = 11{,}000 \pm 500\ s^{-1}$, $\beta(0) = 6{,}780 \pm 530\ s^{-1}$). The kinetic results of Fig. 8 *E* were also used to predict the mean-current vs voltage relationship for BPTI-induced substates in the patch recording. The results plotted in Fig. 8 *F* show that the mean current predicted (*open circles*) from the behavior of $\alpha(V)$ and $\beta(V)$ systematically underestimates the actual measured mean current values (*filled triangles*) unless the small nonzero current pedestal (7% of open-channel current) is taken into account (*solid line*). The results of Fig. 8 thus provide important support for a major assumption underlying the noise analysis of Figs. 3 and 4, that BPTI-induced substate events are the result of a filtered, fast fluctuation between the open and a nearly closed state of the channel.

To examine whether a fluctuating barrier process may also account for the subconductance behavior in-

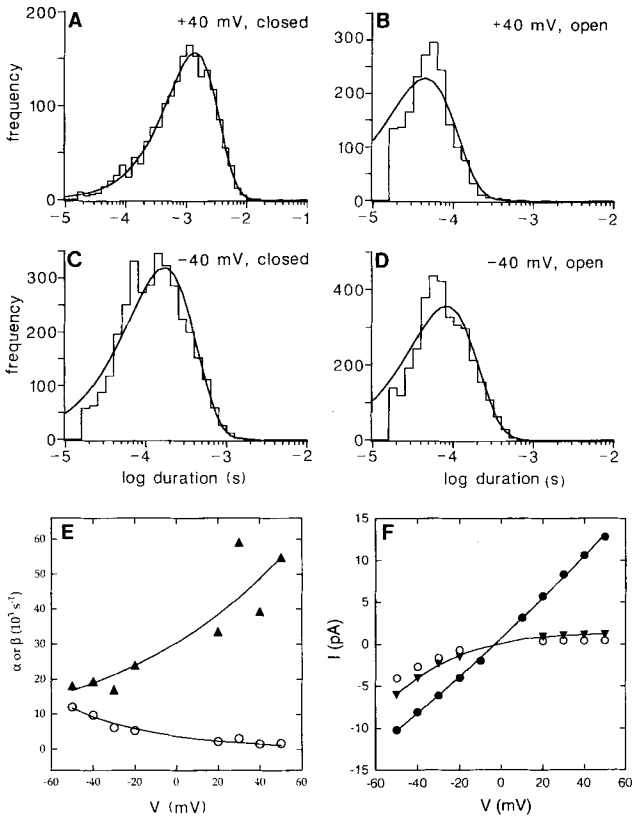

FIGURE 8. Analysis of BPTI-induced substate activity using dwell time histograms compiled from single-channel patch data resolved at 10.5 kHz filtering. (*A* and *C*). Frequency density distribution of closed dwell times during BPTI-induced bursts of activity at +40 mV (*A*, $\tau_c = 1.39$ ms) and −40 mV (*C*, $\tau_c = 0.166$ ms). Full closures were excluded to select only dwell times in the low-conductance pedestal. (*B* and *D*). Frequency density distribution of open dwell times during BPTI-induced bursts at +40 mV (*B*, $\tau_o = 44$ μs) and −40 mV (*D*, $\tau_o = 81$ μs). (*E*) Voltage dependence of rate constants, α (▲) and β (○), respectively, derived from open and closed dwell time histograms after correction for missed events. The data points were fit (*solid lines*) to the equations $\alpha(V) = \alpha(0)\exp(z'_\alpha FV/RT)$ and $\beta(V) = \beta(0)\exp(-z'_\beta FV/RT)$ using $z'_\alpha = 0.30 \pm 0.07$ and $z'_\beta = 0.57 \pm .06$, $\alpha(0) = 30{,}300 \pm 3{,}300\ s^{-1}$ and $\beta(0) = 3{,}690 \pm 390\ s^{-1}$. (*F*) Predicted *I-V* curve for BPTI-induced substate based on the dwell time analysis in comparison to direct measurements of mean current (▼). The predicted points (○) are calculated according to $I_{substate} = I_{open}\,\beta(V)/[\beta(V) + \alpha(V)]$. These latter values fall slightly below the measured mean currents as expected if the contribution of the low-conductance pedestal is ignored. The solid curve is a fit to the substate *I-V* data that takes the pedestal into account by the equation, $I_{substate} = I_{open}\{r + [(1 - r)K(V)/(1 + K(V))]\}$, where $r = I_{pedestal}/I_{open}$, and $K(V) = K(0)\exp(-z'FV/RT)$. Best fit values used to plot this latter function were: $K(0) = 0.19 \pm 0.04$, $z' = 0.95 \pm 0.10$ and $r = 0.07 \pm 0.02$. The *I-V* curve of the fully open state (●) is also shown (slope conductance = 234 pS).

duced by DTX, we analyzed DTX-induced substates recorded at high resolution in patch pipettes. Fig. 9 shows that current records of patch recordings of DTX-induced substates in smooth muscle K(Ca) channels

exhibit excess current noise when filtered at 10.5 kHz. In this case however, the individual opening and closing events responsible for the noise are not resolved, implying that the underlying kinetic process responsible for the DTX-induced substate is faster than accessible at this bandwidth. Using a procedure similar to the analysis of BPTI-substates at 350 Hz (Fig. 3), we fit amplitude histograms of DTX-substates filtered at 5 kHz to a β-distribution to estimate the underlying fluctuation rates (Fig. 10, *A* and *B*). In contrast to the excellent fits of data for the BPTI-substate (Fig. 3), amplitude histograms of the DTX-substate systematically deviated from a theoretical β-function, particularly in the positive voltage range (e.g., Fig. 10 *A*). This appears to be related to difficulties in excluding brief gating closures superimposed on the substate noise and apparent nonstationary behavior within the substate. Nevertheless, the analysis yields transition rates ($\alpha(0) = 115{,}000 \pm 12{,}000\ s^{-1}$, $\beta(0) = 202{,}000 \pm 21{,}000\ s^{-1}$) that are roughly an order of magnitude faster than those measured for the BPTI-substate. The weaker voltage dependence of rate constants measured for the DTX-substate process (Fig. 10 *C*) is consistent with the more weakly rectifying mean *I-V* relation of the DTX-substate (Fig. 10 *D*) as previously documented in bilayer experiments (Lucchesi and Moczydlowski, 1991; Moczydlowski et al., 1992). Thus, the fast fluctuations responsible for the DTX-induced subconductance level ($\tau_\beta \simeq 6$ μs, $\tau_\alpha \simeq 7$ μs at +50 mV) occur on a time scale that is only ~600-times slower than the transit time for K^+ through the open channel at +50 mV (~10 ns).

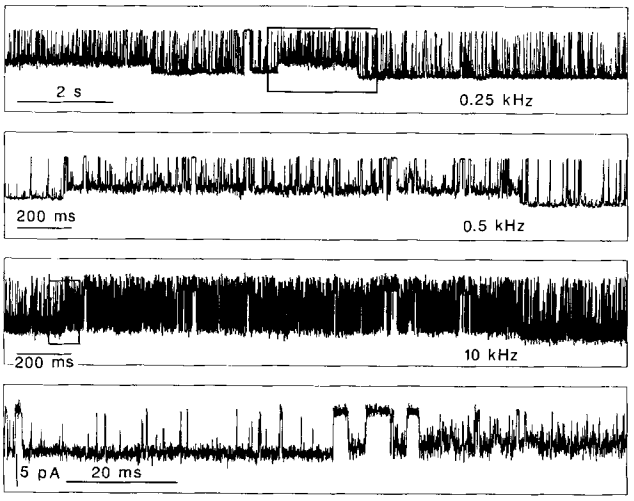

FIGURE 9. High-resolution patch recording of DTX-induced subconductance events in a maxi K(Ca) channel from aortic smooth muscle reveals excess noise. The top trace, filtered at 0.25 kHz shows two long bursts of normal channel openings (downward) at −40 mV interrupted by two DTX-induced substates. The second trace is an expanded segment of data in the first trace marked with a box and filtered at 0.5 kHz. The third trace is the same as the second trace filtered at 10.5 kHz. A boxed segment (third trace) at the transition from a normal opening to a substate is expanded further in the fourth trace.

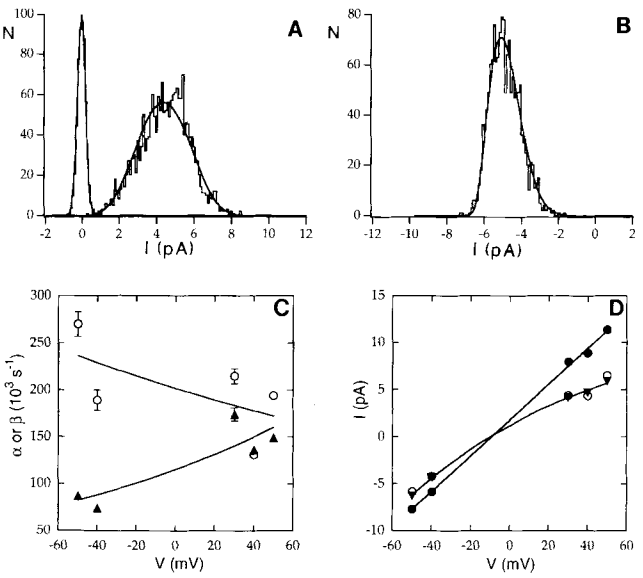

FIGURE 10. Analysis of excess current noise associated with DTX-induced substates using a β-distribution to fit amplitude histograms. (*A*) Amplitude histograms of channel activity at +40 mV separately compiled from complete closures (*left peak*) or DTX-induced substate activity (*right peak*) after filtering at 5.0 kHz. The respective distributions are fit (*solid curves*) to a Gaussian function for the closed state histogram or to a β-function for the substate histogram. (*B*) An amplitude histogram of the DTX-induced substate at −40 mV is fit to a β-function (*solid curve*). (*C*) Voltage dependence of transition rates underlying the DTX-induced substate. Closing rate, α (▲), and opening rate, β (○), were determined from β-function fits as in *A* and *B*. The data points were fit to: $\alpha(V) = \alpha(0)\exp(z'_\alpha FV/RT)$ and $\beta(V) = \beta(0)\exp(-z'_\beta FV/RT)$, using $z'_\alpha = 0.17 \pm 0.06$ and $z'_\beta = 0.08 \pm 0.06$, $\alpha(0) = 115{,}000 \pm 12{,}000\ s^{-1}$ and $\beta(0) = 202{,}000 \pm 21{,}000\ s^{-1}$. Data points correspond to the mean ± SE for four independent measurements. (*D*) Unitary *I-V* curves for the DTX-induced substate and the open channel. Directly measured mean current for the DTX-induced substate (▼) are compared to predictions from β-function analysis (○) as calculated according to: $I_{substate} = I_{open}\ \beta(V)/\{\beta(V) + \alpha(V)\}$. The solid curve through the substate data is fit to the equation in the legend of Fig. 2 using the parameters: $z' = 0.36 \pm 0.05$ and $K(0) = 2.0 \pm 0.2$. The open state *I-V* curve (●) is shown for comparison (slope conductance = 190 pS).

General Effect of Fast Fluctuations on Practical Measurements of Unitary Channel Current

Since many ion channels exhibit excess open-state noise and/or substate noise, it is important to consider the implications of such noise in the molecular interpretation of conductance behavior based on mean unitary *I-V* measurements. To consolidate our findings, we

wished to determine the general relationship between the rate constants for a fast, two-state fluctuation, the filter frequency of a channel recording, and the observed unitary channel current measured by standard amplitude-histogram techniques.

For this purpose, we performed Monte-Carlo simulations of single-channel activity based on a three-state linear kinetic scheme of Closed-Open-Substate as shown in Fig. 11. This scheme was chosen since it generates channel gating transitions between a single closed state and a single open state of defined unitary current (i = 0 and i = 1, respectively), and can be used to explore the effect of a reversible transition to a substate current level, S. The process of generating simulations based on this model is described in Methods. First, a noiseless, unfiltered channel record is simulated using a particular set of rate constants for a Markov process (k, j, α, β). The record is then digitally filtered, Gaussian noise is added, and an all-points amplitude histogram is compiled. Since both the filter frequency and channel dwell-times are defined in units of time set by the sample interval of the digitized data, the natural reduced unit of time for this simulation is the ratio of time over the filter frequency. (For example, simulating 1 s of data with transition rates of 20,000/s filtered at 5,000 Hz is equivalent to simulating 10 s of data with transition rates of 2,000/s filtered at 500 Hz.) Likewise, rate constants and dwell times are defined relative to filter frequency. Thus, the results of these simulations generally apply to the whole domain of rate constants and filter corner frequencies, f, over the range of explored ratios, α/f and β/f.

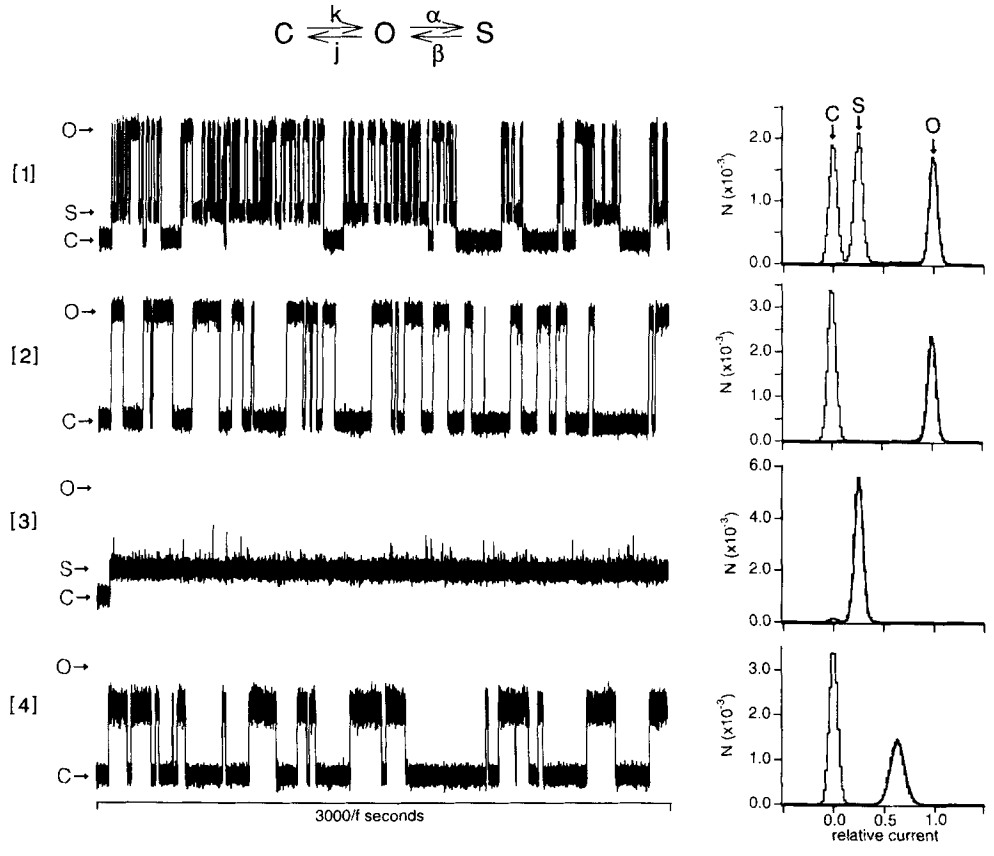

FIGURE 11. Simulation of a model channel that exhibits reversible transitions between the open state and a low-conductance substate. The model channel is assumed to undergo reversible Markovian transitions between three linearly connected states, closed (C), open (O), and substate (S), with rate constants as labeled in the upper kinetic scheme and relative current levels of 0, 1.0, and 0.25, respectively. Single-channel records were generated by Monte Carlo simulation with closed-open (k, j) rate constants held fixed (k = $f/83$, j = $f/50$), while the open-substate (α, β) rate constants relative to a fixed filter corner frequency, f, were systematically varied over a wide range as described in Methods. An all-points amplitude histogram of the simulated data is shown at the right of each trace. The four records shown [*1–4*], correspond to particular examples of limiting behavior as noted at the four corners of the surface plot of Fig. 12. [*1*] $\log(\alpha/f) = -1$, $\log(\beta/f) = -1$. Transitions between the open state and the substate are slow and well resolved, an ideal situation for measuring true unitary current. Three well-resolved peaks in the amplitude histogram at the right correspond to closed state (C), substate (S) and open state (O). [*2*] $\log(\alpha/f) = -0.6$, $\log(\beta/f) = 1.7$. Transitions to the substate are heavily filtered. Dwell times in the substate are rare and brief, whereas dwell times in the open state are well resolved. The substate peak in the amplitude histogram is lost and substate transitions do not significantly affect the estimate of unitary current. [*3*] $\log(\alpha/f) = 1.7$, $\log(\beta/f) = -0.6$. Transitions to the open state are heavily filtered. Dwell times in the open state are rare and brief such that they appear as a slight asymmetry in the current noise. Dwell times in the substate are long and well resolved. Amplitude histogram analysis interprets the substate peak as the apparent open-state level. [*4*] $\log(\alpha/f) = 2$, $\log(\beta/f) = 2$. Transitions between the open state and the substate are very fast such that the filtered record appears to have only one conducting level which is an average of the open state and the substate. The right-most (*open*) peaks in the histograms of [*1–3*] are overlaid with a Gaussian function (*solid curve*) using a standard deviation corresponding to that of the closed level noise. The right-most peak in [*4*] is overlaid with a fit to a β-function (*solid line*).

For the simulations we have chosen to present, the substate current level was fixed at 0.25 of the open channel current level. This low substate level was chosen to approximate the low current pedestal observed for the BPTI-substate phenomenon and to allow for clean separation of histogram peaks of the three levels in the case of slow rate constants relative to f. Gaussian noise ($\sigma = 0.05$ of open-channel current) was added after filtering because the background noise in single-channel recordings is typically Gaussian. Since the power spectrum of instrumental or background noise depends upon the recording method and amplifier, specific applications of this method would require knowledge of the background noise characteristics of the particular recording system. By adding noise after filtering, our simulations focus on the intrinsic contribution of the substate process to the appearance of amplitude histograms. The results can be readily extrapolated to different values of the substate level, S, by appropriately scaling the relative values of S and the open-state current.

As described in Methods, the slow channel gating rate constants (k, j) were held fixed by the simulation program while the rate constant ratios, α/f and β/f, were systematically varied over four orders of magnitude from 10^{-1} to 10^{2}, thus exploring all combinations of rate constants for the substate process ranging from 0.1 to 100 times the filter frequency. The resulting amplitude histogram was used to estimate the apparent open-channel current by criteria described in Methods. Fig. 12 *A* is a three-dimensional surface plot of the apparent open-channel current shown on a linear scale as a function of the closing (α/f) and opening (β/f) rate constant ratios on a logarithmic scale.

To understand the shape of this surface plot, first consider behavior at, or near points at the four corners labeled *1–4* as shown in Fig. 11. In trace *1* of Fig. 11, $\log(\alpha/f)$, $\log(\beta/f) = -1, -1$, all transition rates are slow relative to the filter frequency, and dwell times in all states of the channel are well resolved. In this case, the program correctly identifies the true open-channel current level as the right-hand peak of the amplitude histogram. For the second case of trace *2*, where $\log(\alpha/f)$, $\log(\beta/f) = -0.6, 1.7$, closing events from the open state to the substate are so brief that, after filtering, there are virtually no resolved transitions to the substate. Under these conditions, the substate process makes practically no contribution to the channel record and the program readily selects the right-hand peak of the amplitude histogram as the true open-channel current. At the third corner of the surface plot (Fig. 11 *A*, trace *3*), the situation is reversed from that of case *2*. The probability of the channel being in the fully open state is quite low. The channel spends most of the time that it is not closed in the substate with a few, brief transitions to the fully open conductance level. In this case, the program identifies the substate current level at 0.25 as the apparent open-channel current. Finally, in trace *4* transitions between the substate and the open state are very fast and unresolved ($\log(\alpha/f)$, $\log(\beta/f) = 2, 2$). In this case, the simulated record exhibits a single conducting level with slightly excessive

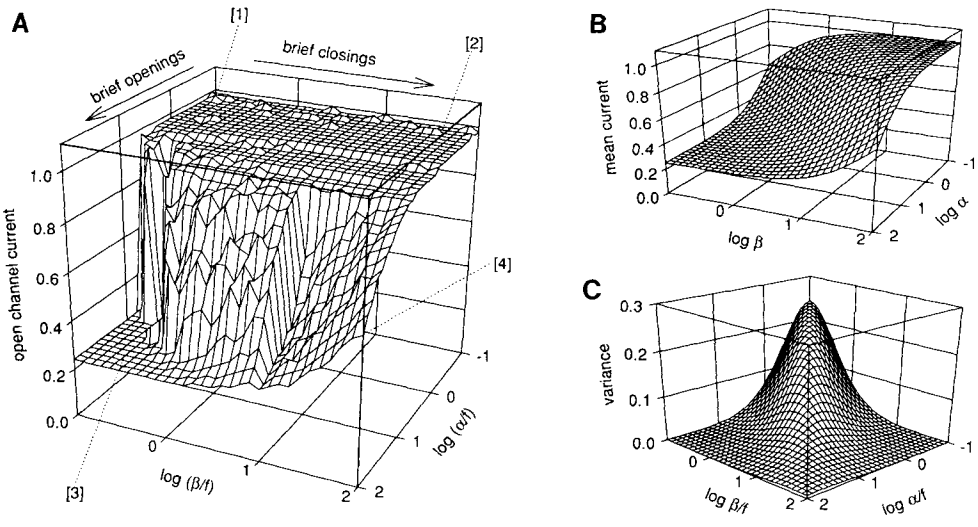

FIGURE 12. Characterization of the failure of amplitude histograms to report true unitary current when the closing rate leading to a subconductance state is fast relative to the filter frequency. (*A*) Surface plot of apparent open-channel current (in arbitrary units) as a function of the logarithm of transition rates, α and β, relative to filter corner frequency, f, for the scheme given at the top of Fig. 11. Open-channel current for simulated data at each point was measured with the use of an automated amplitude-histogram program described in Methods. Dotted lines at the corners of the plot indicate the positions of four types of limiting behavior, [*1–4*], as shown in Fig. 11. (*B*) Surface plot of mean current, $\langle i \rangle$, within a long burst of open-substate events as a function of the logarithm of transition rates, α and β, calculated according to $\langle i \rangle = (\beta + s\alpha)/(\beta + \alpha)$, where s, the fractional current of the substate, is equal to 0.25. (*C*) Surface plot of theoretical current variance (in arbitrary units squared) due to open-substate (O-S) transitions, after filtering with a Gaussian filter, over the same range of rates relative to filter frequency shown in plot (*A*). Variance was calculated as described in Materials and Methods.

noise, that is actually an average of the substate and open-state current level. In this situation, the program identifies the peak of this average current level centered at 0.625 as the apparent open-channel current. The amplitude distribution of this apparent conductance level for trace *4* conforms to a β-distribution under appropriately filtered conditions as observed for the maxi K(Ca) channel substates induced by DTX and BPTI. It is worth noting, that in this extreme case of $\alpha/f = \beta/f$, the amplitude distribution is nearly Gaussian (Yellen, 1984) and may be interpreted as a broad Gaussian distribution.

Having considered the limiting behavior at the four corners of the plot in Fig. 12 *A*, the behavior of the rest of the plot can be readily understood. The surface plot consists of several distinct regions. First, there is a large plateau of current values near ~1.0 that extends over the region defined by $\log(\beta/f) = -1$ to $+2$ and $\log(\alpha/f) = -1$ to ~0.9. In this region, the amplitude histogram method is fairly reliable because open-state dwell times are either fully resolved, or close to being resolved. However, as $\log(\alpha/f)$ exceeds this range, open-state dwell times become short and unresolved, and the simulation program attempts to identify the longest brief openings in the open-current level by fitting a half-Gaussian function to the tail (right-hand edge) of the amplitude histogram. This results in an underestimation of the true open-channel current level and accounts for the steep fall in the estimated value of open-channel current in the region bounded by $\log(\beta/f)$ from -1 to ~1, and $\log(\alpha/f) > 1$. Examples of simulations in this region are shown in Fig. 13 (*top three records*). In these records, there are many brief, unresolved transitions to the open state and the program either interprets the substate level as the open state (Fig. 13, *top record*) or uses the long tail of the highly skewed amplitude histogram to estimate the highest open-state level (Fig. 13, second and third trace from top). The region of Fig. 12 *A* bounded by $\log(\alpha/f) > 1$ and $\log(\beta/f) > 1$ closely corresponds to a β-function. In this region, exemplified by bottom two records of Fig. 13, the simulation program identifies the peak of the amplitude histogram as an estimate of the open-channel current. Because there is a sharp transition between estimation methods (tail of the histogram vs the peak bin) at the validity limit of the β-function, there is also a sharp transition in this region of the plot (Fig. 12 *A*), reflecting a problem of decision making, that resembles a right-angled cliff.

In explaining the behavior illustrated in Fig. 12 *A*, it is instructive to compare this plot with the corresponding surface plot in Fig. 13 *B* of the mean current level within a burst of substate activity as defined by periods that the channel spends in the grouped open state (O) and substate (S) before it enters a long closure to the C state. The mean current, $\langle i \rangle$ in the grouped (O, S) state, is given by a weighted mean, $\langle i \rangle = (\beta + s\alpha)/(\beta + \alpha)$, where *s*, the relative substate current, is equal to 0.25 in the present example. The mean current is independent of filter frequency since filtering only distorts the observed time response, not the underlying equilibrium. As expected, in the limit of heavy filtering, represented by the edges, $\log(\alpha/f) = 2$ and $\log(\beta/f) = 2$, the behavior of Fig. 12 *A* converges to that of Fig. 12 *B*. Thus, the simulation results serve to reinforce the basic fact that filtering is a form of averaging and a filtered signal represents the average behavior of the underlying process.

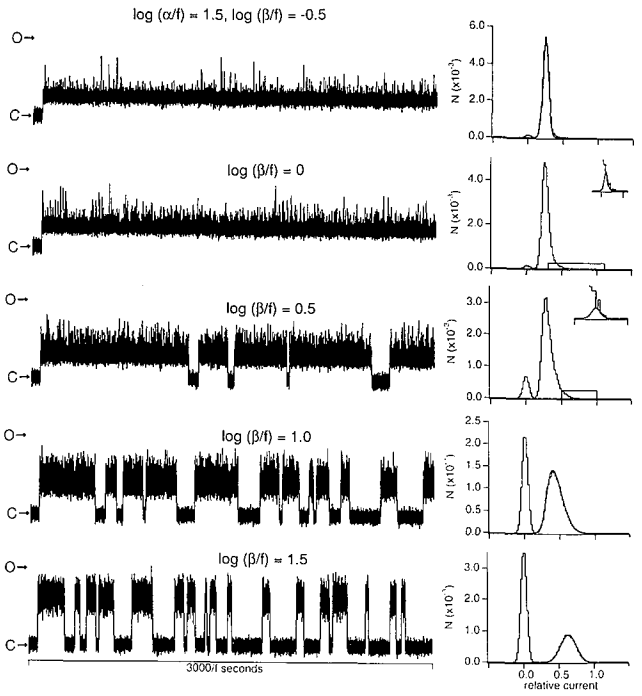

FIGURE 13. Simulations of single-channel data and amplitude histograms corresponding to a "slice" through the plot in Fig. 12 *A* in a region of rapid transitions to the substate. The five simulations use the same rate constant for entering the substate, $\log(\alpha/f) = 1.5$. From top to bottom, the opening rate is sequentially incremented by 0.5 log units starting from $\log(\beta/f) = -0.5$. This series illustrates the increase in apparent open-state current as the channel spends more time in the open state relative to the substate. True open (*O*) and closed (*C*) levels are indicated by arrows at the left of each simulated trace. In the topmost trace, the automated analysis program judges opening transitions from the substate as too infrequent and brief to attempt to correct for the slightly skewed histogram of the apparent open state. The program fits a Gaussian function (*solid curve*) to the amplitude peak centered at the substate. In the second and third traces, the program detects a skewed distribution and estimates the open-current level by superimposing a Gaussian curve along the right hand edge of the amplitude distribution as magnified in the insets. In the bottom two traces, amplitude distributions for the open level are fit with a β-function (*solid lines*).

What conclusions can be drawn from Fig. 12 regarding subconductance behavior induced in the maxi K(Ca) channel by BPTI and DTX? First, this analysis shows that true open channel current can be correctly identified from the open state peak of an amplitude histogram as long as the fastest closing transition rate, α, is less than $\sim$10 times the filter frequency ($\log(\alpha/f) < 1$) as indicated by the large plateau of safe area in Fig. 12 *A* where current values are $\simeq$1. Above this range of α/f, the true unitary current may be greatly underestimated by relying on measurements of apparent current levels. Within a steep 10-fold range of α/f from $\sim$10 to 100, a standard level-based estimate of open-channel current rapidly converges to the mean current level of a fluctuating process. The front-most cliff or "waterfall" in the surface plot of Fig. 12 *A* thus defines a "danger zone" for the measurement and interpretation of unitary conductance and subconductance behavior. The apparent substates induced by BPTI and DTX that we have recorded under different conditions of resolution and filtering undoubtedly reflect the behavior at or beyond this cliff region of Fig. 12 *A* rather than a change in a static energy profile for K^+ conduction. For example, the BPTI-substate recorded in bilayers at +50 mV and 500 Hz filtering (Fig. 3, *top record*) corresponds to $\log \alpha/f = 1.6$, $\log \beta/f = 0.73$ and closely resembles the simulated records in this region shown in Fig. 13.

The recognition that filtered single-channel currents underestimate true unitary current may be considered trivial when excess noise can be readily resolved. However, in situations such as simulation *4* in Fig. 11, the excess noise is very slight and yet the apparent conducting state of the channel is 37.5% less than the true open current. This particular situation is not unusual in practical analysis applications. For example, the DTX-substate recorded in bilayers at −40 mV and 500 Hz filtering (Fig. 9, *second trace from top*) corresponds to $\log \alpha/f = 2.2$, and $\log \beta/f = 2.7$. This example lies in the limiting region just outside the simulation range for high ratios of α/f and β/f explored in Fig. 12 *A*. In such situations, slightly excessive open-state noise is routinely ignored in constructing open channel *I-V* relations. This problem is illustrated by the relationship plotted in Fig. 12 *C*. This latter surface plot shows the theoretical variance of a filtered two-state (open-closed) process as a function of the transition rates. Along the diagonal of this plot (where $\alpha/f = \beta/f$), the variance of an unfiltered signal, as given by the formula, $\sigma^2 = P_{open}(1\text{-}P_{open})i^2$ (Sigworth, 1980), is constant and equal to 0.25 (using $P_{open} = 0.5$, $i = 1$). However, filtering causes the observed variance to drop sharply along this diagonal with increasing transition rates and to approach that of the background noise. Thus, the observed amplitude of excess noise is not necessarily a reliable indication of whether a single-channel current measurement reflects the intrinsic unitary current of the open-pore conformation.

DISCUSSION

Identification of a Fluctuating-Barrier Process as a Mechanism for Substate Production

The major new finding of this paper is that subconductance behavior induced in maxi K(Ca) channels by the small, homologous proteins, BPTI and DTX, is due to rapid fluctuations of the open channel. This mechanism for substate production was previously proposed by Dani and Fox (1991) as a way to explain the common observation that substates of ion channels often exhibit the same ionic selectivity and ion-binding affinity as the primary open state (Labarca and Miller, 1981; Tomlins et al., 1984; Fox, 1987; Hill et al., 1989). Fluctuating barrier theory of ion permeation is also supported by the work of Läuger, Sigworth, and others who developed key concepts and experimental evidence in favor of the idea that dynamic motion of channel proteins may produce open-channel noise on a variety of time scales that influences the process of ion permeation (Läuger et al., 1980; Läuger, 1983, 1985; Sigworth, 1985; Heinemann and Sigworth, 1990, 1991, 1993). To our knowledge, the present example is the first case where this mechanism has been found to be the underlying basis of current-voltage rectification at the single-channel level, as previously proposed on theoretical grounds (Läuger, 1985; Eisenman, 1987).

This conclusion is supported by several lines of evidence including experiments that rule out a simple block of the channel pore and the independent observation of excess noise associated with the subconductance states. From past work, it is clear that BPTI and DTX do not directly block the internal mouth of the channel as shown by a lack of competition with the internal pore blockers, Ba^{2+} and TEA (Lucchesi and Moczydlowski, 1991). In contrast, the internal blocking action of the *Shaker* inactivation "ball" peptide on maxi K(Ca) channels is strictly competitive with internal TEA (Toro et al., 1992; Foster et al., 1992). Thus, these two classes of protein inhibitors of the maxi K(Ca) channel must act from the internal side by very different mechanisms. The observation of a low conductance pedestal (Fig. 8) during the BPTI substate supports the notion that the entrance to the pore is not physically blocked and explains why TEA and Ba^{2+} can readily access their binding sites in the permeation pathway during the BPTI substate. Secondly, an increase in K^+ concentration or ionic strength from 50 to 500 mM does not relieve the relative substate current, although the BPTI/DTX association rate is strongly suppressed (Lucchesi and Moczydlowski, 1991). This indicates that

once BPTI/DTX is bound, the process responsible for the lower mean current is not easily reversed by increased occupancy of the channel by K^+ or by higher ionic strength. Again, this implies that the BPTI/DTX molecule itself does not directly interfere with permeation by a fast blocking process (e.g., rapid movement of a lysine group into and out of the pore) or by electrostatic reduction of local K^+ concentration (i.e., surface charge effect, Latorre et al., 1992), since both types of inhibition would be expected to be relieved by an increase in ionic strength. If BPTI and DTX do not interfere directly with ion permeation, they must do so indirectly.

Here we have found that the apparent substate is not simply a reduction in unitary current through the open channel as predicted by a "static" model of ion permeation in which the pore changes to a different conformation with a less favorable energy profile. Rather, the substate is due to rapid switching between the open state of the channel and a nearly closed state. In the case of BPTI, this fluctuating-barrier process is revealed by excess noise observable in the range of 100–500 Hz that is well-described by a β-distribution for a filtered two-state process (Fig. 3). The underlying rate constants derived for this fluctuation (α, β) follow exponential functions of voltage that account for the inward rectification of the mean *I-V* relation of the substate (Fig. 4). The assumption that the β-distribution results from a two-state process was tested by extending the resolution of the BPTI substate for a different species of maxi K(Ca) channel to 10.5 kHz using patch-pipette recording. This revealed incomplete closures during the BPTI substate (~10–15% of the open-state current, Fig. 7) but resolved exponentially distributed open and closed dwell times with the expected voltage-dependence (Fig. 8). Finally, we found that the homologous protein, DTX, also acts by a fluctuating barrier mechanism as demonstrated by excess noise observed at high resolution (Fig. 9) and similar approximation of amplitude histograms of this substate by a β-distribution (Fig. 10).

In discussing this phenomenon, we have assumed that BPTI and DTX act by binding at the same site or sites on the K(Ca) channel. This is expected from their sequence identity (~30%) and similar three-dimensional structure (Skarzynski, 1992). In support of this, we have found that DTX and BPTI do exhibit competitive binding interactions when assayed at the single-channel level (Moczydlowski et al., 1992; G. Moss, unpublished results), although these data have not yet been analyzed quantitatively. The number and location of binding sites for DTX/BPTI on K(Ca) channels is an important question for future work, given the presumed tetrameric subunit structure of maxi K(Ca) channels as the product of slowpoke-related genes and distant relatives of the tetrameric K_V-channel superfamily of proteins (Shen et al., 1994).

Another important question is whether the substate phenomenon mediated by BPTI/DTX is merely an interesting model of open-channel noise or whether there are physiological correlations of this behavior? One possible correlation is the recent finding that brief flicker closures (<50-μs duration) of native maxi K(Ca) channels close to a subconductance level that is 5–10% of the open-channel current (Ferguson et al., 1993). This same study also found that longer closures of the native channel close very transiently to a similar current sublevel before closing completely. The incomplete closures of the native channel described by Ferguson et al. (1993) resemble closures at the low-conductance pedestal observed here for the BPTI-bound channel (Fig. 7). It is possible that rapid current fluctuations of the BPTI-bound channel reflect conformational changes similar to those of the normal channel. The native channel has also been found to exhibit rare "buzz modes" of low open state probability with a very brief mean open time of 50 μs (McManus and Magleby, 1988). This buzz mode of the native channel bears a strong resemblance to highly resolved BPTI-substates and it is possible that they share a common underlying mechanism.

Simulation of a Rapidly Fluctuating Two-State Process Defines a Critical Zone Where Amplitude Histograms Fail to Accurately Report True Single-Channel Current Levels

It is well known that filtering limits the resolution of brief current steps. Several studies have considered the quantitative impact of this problem on the 50% threshold method for measuring dwell times at the single-channel level. To address this problem, various approaches have been devised for the correcting dwell time histograms for errors due to missed events arising from limited recording bandwidth (Colquhoun and Sigworth, 1983; Blatz and Magleby, 1986; McManus et al., 1987; Milne et al., 1989; Crouzy and Sigworth, 1990; Wonderlin et al., 1990*b*). However, relatively less attention has been given to similar errors encountered in the measurement of filtered unitary current amplitudes with the use of amplitude histograms. The most commonly used method for measuring single-channel current is to filter the record at a bandwidth that attenuates most of the high-frequency background noise, compile an amplitude histogram, and identify a peak corresponding to the open-channel current. Motivated by our experience in measuring BPTI-induced substate events under a variety of filtering and noise conditions, we carried out a general simulation of the effect of a fast, two-state fluctuation on unitary current measurement based on the use of amplitude histograms.

When considering the implications of our results, it is important to realize that the methods our program uses to measure apparent unitary currents are based on

practical techniques described in the literature. Thus, we believe that Fig. 12 *A* represents a fair approximation of worst case underestimates of true unitary current that may occur when special care is not taken to assess excess current noise. The basic conclusion from this simulation is that a serious underestimation (>5% error) of current amplitude can occur whenever there is a closing rate constant leading from an open state that is greater than eight times the filter cutoff frequency, *f*. This result is analogous to the deadtime formula for measuring dwell times: events shorter than a deadtime, T_d, are missed completely at the 50% threshold detection limit when they are ~1/5.6 times the reciprocal filter frequency, $T_d = 0.179/f$ (Colquhoun and Sigworth, 1983). A more specific examination of the reasons for the failure of amplitude histograms at high transition rates (relative to *f*) shows that it is difficult to detect and accurately evaluate the amplitude tail of a highly skewed histogram. Also, in the limit of fast closing and opening fluctuations, a β-distribution of excess noise mimics a Gaussian distribution expected for the background noise.

Several methods have been previously described for correcting measurements of single-channel current amplitudes, but none of these are fail-safe. The most straightforward approach is to directly fit the time course of individual opening and closing events to match the filtered response of the recording system (Colquhoun and Sigworth, 1983; Ferguson et al., 1993). However, as noted by Colquhoun and Sigworth (1983), for events much shorter than the recording system risetime, it becomes very difficult to simultaneously find the correct duration and amplitude that fits an attenuated pulse. In a specific application of measuring the unitary current of single voltage-sensitive K-channels, Wonderlin and French (1991) introduced a tail-fit method for estimating the highest genuine current amplitude of the population. However, as applied to the simulation of Fig. 12, we find that this method ultimately fails to measure the true amplitude in the limit of brief openings. Beta-function analysis is a very useful method for extending the resolution of brief dwell times to values below the system deadtime (FitzHugh, 1983; Yellen, 1984), but practical applications of this method generally assume that the underlying current amplitudes of the two-state process are known or they are equated with resolved states of the current record. It may be expected that simultaneous fitting of both amplitudes and dwell times (four parameters) to binned data with a β-distribution would lead to a range of acceptable fits with some uncertainty in the estimated amplitudes (e.g., Nakazawa and Hess, 1993). Similar difficulties at the high frequency limit undoubtedly apply to analogous approaches such as higher-order cumulants of the amplitude distribution (Heinemann and Sigworth, 1991) and the analysis of power spectra (Heinemann and Sigworth, 1993).

Therefore, it must be recognized that measurement of a unitary current, whether it is defined as an open state or a substate, is an apparent value that is a function of the filter frequency of the observation. For this reason, a critical evaluation of excess noise is an important task in defining the mechanism of ion conduction. This requires an effort to collect single-channel data at the best possible resolution (low background noise, high filter frequency). If little excess noise is present at the highest achievable resolution, then confidence in any static model of ion permeation is proportionally greater. However, if excess noise is associated with a particular conductance level and it cannot be attributed to a direct blocking process, then the contribution of a fluctuating barrier mechanism merits consideration.

Other Examples of Open Channel Noise and Possible Implications

Theory suggests that protein conformational changes on the time scale of ion transport can have profound implications for interpreting the conductance behavior of channel proteins (Läuger et al., 1980; Ciani, 1984; Eisenman and Dani, 1986; Eisenman, 1987; Mironov, 1992). In particular, these latter studies have noted that fluctuating barrier models involving reversible changes in affinity at a single ion-binding site can generate behavior that is usually attributed to multi-ion occupancy. Such behavior arises from the coupling of ion transport to protein conformational changes and can occur when the rate of conformational fluctuations is equal to or less than the rate of ion translocation steps (Läuger et al., 1980; Läuger, 1985; Eisenman and Dani, 1986). Despite this awareness, there have been relatively few studies of open-channel noise for most of the major classes of physiologically significant channels. In the few cases where it has been investigated, evidence indicates that structural fluctuations may be quite important.

For example, unitary ionic currents of the low molecular weight gramicidin channel display very little excess noise below the measurable range of 20 kHz and can generally be well described by rigid pore models of transport. However, Cs^+ currents through gramicidin channels do exhibit excess open-state noise corresponding to current interruptions of ~1 μs (Heinemann and Sigworth, 1991). This noise has been attributed to fluctuations in the entry barriers for Cs^+ and is speculated to arise from motions of the carboxyl-terminal residue at the channel mouth (Heinemann and Sigworth, 1990). This latter study suggests that the binding of Cs^+ stabilizes a relatively more open conformation of

gramicidin. Gramicidin channels have also been found to exhibit subconductance behavior due to structural perturbations at the dimer interface (Oiki et al., 1992), suggesting that inter-subunit interactions may also be an important determinant of open-channel noise.

Unitary currents of rat muscle Ach-receptor channels have been found to exhibit low-frequency, open-state noise consistent with a current fluctuation of 3% of the open-channel amplitude on a time scale of ~1 ms (Sigworth, 1985). The relatively high temperature dependence of this process ($Q_{10} \sim 3$) implies that it reflects a conformational fluctuation rather than a diffusional process. This particular type of low frequency fluctuation can be explained by random transitions among many closely spaced conductance levels (Heinemann and Sigworth, 1993). Native Ach-receptor channels from cultured chick muscle cells also display a prominent substate level that has a significantly larger variance than the main open state, suggesting that some type of fluctuation underlies the substate level (Auerbach and Sachs, 1984). Single K channels of skeletal muscle and heart sarcoplasmic reticulum (SR) exhibit a prominent subconductance state that displays the same ionic selectivity as the main open state (Labarca and Miller, 1981; Tomlins et al., 1984; Fox, 1985; Hill et al., 1989). Hill et al. (1990) noted that current noise of the SR K-channel substate recorded in bilayers is significantly greater than that of the open state at a bandwidth of 100 Hz. These authors proposed a flutter model involving a weighted average of two current levels as the basis for the substate. Recently, Hainsworth et al. (1994) characterized excess open-state noise in SR K-channels from native lobster SR and concluded that motions of the channel molecule in the range of 10^4–10^7 Hz are a likely source of this behavior.

In addition to these examples, the single-channel literature holds numerous observations where consideration of fluctuating barrier models could potentially yield new insights. One application concerns the mechanistic interpretation of unitary *I-V* relations that rectify under conditions of symmetrical permeant ion concentration. Specifically, single-channel *I-V* curves of various Cl channels exhibit outward rectification in the presence of symmetrical Cl^- solutions (Welsh and Liedtke, 1986; Chen et al., 1989; Lukacs and Moczydlowski, 1990). Similarly, unitary *I-V* relations of a number of voltage-sensitive K-channels also exhibit moderate inward rectification in the presence of symmetrical K^+ (Isacoff et al., 1991; Wonderlin and French, 1991). Other notable examples of strongly rectifying conductance states have also been described for a plant K^+ channel (Tyerman et al., 1992) and a bacterial anion-selective channel (Schurholz et al., 1993). An attractive explanation for these observations is a voltage-dependent fluctuating barrier process similar to that described here. If such examples of rectification cannot be attributed to possible blocking ions such as Ca^{2+}, Mg^{2+}, and H^+, or the presence of asymmetric surface potentials, then investigation of the possible voltage dependence of open-channel noise is warranted.

Another relevant question concerns observed differences in the unitary conductance of channel isoforms that are members of a closely related gene family. For example, L, N, and T-type Ca-channels display apparently different unitary current amplitudes (Nowycky et al., 1985); and, similar variations in unit conductance occur for homologous members of the K_V channel family (Stühmer et al., 1989) when compared at ~1 kHz bandwidth. In some cases, such differences have been attributed to particular amino acid substitutions in the pore-forming domains (Taglialatela et al., 1993). Another way to explain apparent conductance differences among channel isoforms would be to propose that structurally related channels have approximately the same intrinsic open-state current but differ in the equilibrium constant of a fast filtered fluctuation, as modeled in Fig. 12. This idea would predict that channel relatives may display dramatic differences in open-state noise at an appropriate bandwidth. A case of particular interest is the observation that distinct gating modes of a single N-type Ca-channel also differ in unitary current by ~0.2 pA (Delcour et al., 1993). In light of our findings, it is possible that both gating modes of this channel actually have the same open-state current, but a shift in equilibrium of a fluctuating barrier process gives rise to different observed current levels. Hidden, fast fluctuations may be of general importance to the superfamily of voltage-sensitive ion channels since voltage-sensitive Na-channels also exhibit prominent subconductance behavior in the presence of drugs that prolong inactivation (Patlak, 1993).

Other cases of ligand-induced substates may ultimately be explained by fluctuating barrier theory. One example to be considered is the dramatic effect of the alkaloid, ryanodine, on the SR Ca-release channel. This channel normally exhibits a very complicated pattern of gating activity and binding of ryanodine appears to "lock" the channel at a stable ~40% subconductance level (Lindsay et al., 1994). As we have seen here, a fluctuating barrier model predicts that ligand-induced substates may either exhibit more or less excess noise than the unmodified channel, depending on the change in rate constants relative to filter frequency. Other candidate phenomena include the effect of lipophilic alkaloid toxins, such as batrachotoxin and veratridine, on voltage-sensitive Na-channels (Correa et al., 1991; Wang et al., 1990; reviewed in Moczydlowski and Schild, 1994) and an oxygen-dependent change in unitary conductance of a large conductance Ca^{2+}-activated K channel in rat brain neurons (Jiang and Haddad, 1994).

As some of the preceding examples suggest, open channel noise and fluctuating barriers also have implications for the analysis of channel gating (i.e., broadly defined as the kinetic pathway by which channels open and close). If the open current level is inherently noisy, then brief transitions detected at high bandwidth could arise from an unresolved process with an unknown conductance substructure. This leads to an inevitable duality in the classification of events attributable to the gating process vs those assigned to the conduction process. This duality is an inherent feature of Läuger's original model (Läuger et al., 1980) and predicts coupling between pore occupancy and channel gating that has been documented in a number of cases, including maxi K(Ca)channels (Swensen and Armstrong, 1981; Matteson and Swenson, 1986; Miller et al., 1987; Richard and Miller, 1990; Neyton and Pelleschi, 1991; Demo and Yellen, 1992). In our simulations of the linear Closed-Open-Substate scheme, one of the ways such coupling can originate is apparent from the variation in the probability of the long-lived closed (C) states in records of Figs. 11 and 13. As the dwell time in the Substate increases (decreasing β/f), it appears that the channel has a lower unitary conductance but it closes less frequently. This is because there is no direct pathway between the Closed state and the Substate in the scheme we have assumed. As the probabilty of residing in the subconductance state increases, the probability of channel closing decreases. When the substate is favored, the slow gating equilibrium (C-O reaction) of the channel appears to shift toward an open state with lower apparent conductance but higher "open" probability. Thus, apparent changes in gating kinetics can occur if ion occupancy of the channel alters the conformational equilibrium between open and unresolved conductance states.

Conclusion

Our pursuit of the mechanism of interaction of Kunitz inhibitor/dendrotoxin proteins with maxi K(Ca) channels has forced us to look beyond static, photographic images of channel pores and seriously consider the implications of protein dynamics. The example of BPTI- and DTX-induced substates supports the notion that rapid protein conformational transitions underlying open-channel noise can have a substantial influence on the process of ion conduction. Another implication concerns the interpretation of mutational studies of channel domains involved in permeation. Our results suggest that apparent changes in unitary conductance caused by a mutation could result from indirect allosteric effects that perturb fluctuating barrier processes rather than direct chemical interactions between pore-lining residues and permeant ions. Despite the danger of interpreting mutations, a mutational approach to the identification of structural domains of maxi K(Ca) channels that mediate the BPTI effect may help to elucidate the physical nature of the fluctuating barrier we have invoked to explain conductance and rectification changes.

This paper is dedicated to the memory of Peter Läuger in recognition of his contribution to channel biophysics.

We thank Fred Sigworth (Yale University) for extensive help and encouragement, for suggesting the application of the β-distribution, for sharing computer equipment and software, and for critically reviewing an early version of the manuscript. We also thank Owen McManus (Merck Research Laboratories) for providing smooth muscle cells and Alan Harvey (University of Strathclyde) for DTX.

Supported by Brown-Coxe and Donaghue Foundation fellowships (G. Moss) and National Institutes of Health grant GM-51172.

Original version received 19 April 1995 and accepted version received 2 June 1995.

REFERENCES

Alvarez, O., A. Villarroel, and G. Eisenman. 1992. Calculation of ion currents from energy profiles and energy profiles from ion currents in multibarrier, multisite, multioccupancy channel model. *Methods Enzymol.* 207:816–854.

Andersen, O. S., W. N. Green, and B. W. Urban. 1986. Ion conduction through sodium channels in planar lipid bilayers. *In* Ion Channel Reconstitution. C. Miller, editor. Plenum Publishing Corp., NY. 385–404.

Auerbach, A., and F. Sachs. 1984. Single-channel currents from acetylcholine receptors in embryonic chick muscle. Kinetic and conductance properties of gaps within bursts. *Biophys. J.* 45:187–198.

Blatz, A. L., and K. L. Magleby. 1986. Correcting single channel data for missed events. *Biophys. J.* 49:967–980.

Bracewell, R. N. 1965. The Fourier transform and its applications. McGraw-Hill, NY.

Caceci, M. S., and W. P. Cacheris. 1984. Fitting curves to data: the Simplex algorithm is the answer. *BYTE.* 340–362.

Cecchi, X., D. Wolff, O. Alvarez, and R. Latorre. 1987. Mechanisms of Cs^+ blockade in a Ca^{2+}-activated K^+ channel from smooth muscle. *Biophys. J.* 52:707–716.

Chen, J. H., H. Schulman, and P. Gardner. 1989. A cAMP-regulated chloride channel in lymphocytes that is affected in cystic fibrosis. *Science (Wash. DC).* 243:657–660.

Ciani, S. 1984. Coupling between fluxes in one-particle pores with fluctuating energy profiles: a theoretical study. *Biophys. J.* 46:249–252.

Colquhoun, D., and F. J. Sigworth. 1983. Fitting and statistical analysis of single-channel records. *In* Single Channel Recording. B. Sakmann and E. Neher, editors. Plenum Publishing Corp., NY. 191–263.

Correa, A. M., R. Latorre, and F. Bezanilla. 1991. Ion permeation in normal and batrachotoxin-modified Na^+ channels in the squid giant axon. *J. Gen. Physiol.* 97:605–625.

Creighton, T. E., and I. G. Charles. 1987. Biosynthesis, processing and evolution of bovine pancreatic trypsin inhibitor. *Cold Spring Harbor Symp. Quant. Biol.* 52:511–519.

Crouzy, S. C., and F. J. Sigworth. 1990. Yet another approach to the dwell-time omission problem of single-channel analysis. *Biophys. J.* 58:731–743.

Dani, J. A., and J. A. Fox. 1991. Examination of subconductance levels arising from a single ion channel. *J. Theor. Biol.* 153:401–423.

Delcour, A. H., D. Lipscombe, and R. W. Tsien. 1993. Multiple modes of N-type calcium channel activity distinguished by differences in gating kinetics. *J. Neurosci.* 13:181–194.

Demo, S. D., and G. Yellen. 1992. Ion effects on gating of the Ca^{2+}-activated K^+ channel correlate with occupancy of the pore. *Biophys. J.* 61:639–648.

Eisenman, G. 1987. Electrical signs of rapid fluctuations in the energy profile of an open channel. *In* IonTransport Through Membranes. K. Yagi and B. Pullman, editors. Academic Press, NY. 101–129.

Eisenman, G., and J. A. Dani. 1986. Characterizing the electrical behavior of an open channel via the energy profile for ion permeation: a prototype using a fluctuating barrier model for the acetycholine receptor channel. *In* Ionic Channels in Cells and Model Systems. R. Latorre, editor. Plenum Publishing Corp., NY. 53–87.

Ferguson, W. B., O. B. McManus, and K. L. Magleby. 1993. Opening and closing transitions for BK channels often occur in two steps via sojourns through a brief lifetime subconductance state. *Biophys. J.* 65:702–714.

FitzHugh, R. 1983. Statistical properties of the asymmetric random telegraph signal, with applications to single-channel analysis. *Math. Biosci.* 64:75–89.

Foster, C. D., S. Chung, W. N. Zagotta, R. W. Aldrich, and I. B. Levitan. 1992. A peptide derived from the *Shaker* B K^+ channel produces short and long blocks of reconstituted Ca^{2+}-dependent K^+ channels. *Neuron.* 9:229–236.

Fox, J. A. 1985. Conductance and selectivity properties of a substate of the rabbit sarcoplasmic reticulum channel. *Biophys. J.* 47:573–576.

Fox, J. A. 1987. Ion channel subconductance states. *J. Membr. Biol.* 97:1–8.

Freund, J. E. 1971. Mathematical Statistics. 2nd edition. Prentice-Hall, Englewood Cliffs, NJ.

Hainsworth, A. H., R. A. Levis, and R. S. Eisenberg. 1994. Origins of open-channel noise in the large potassium channel of sarcoplasmic reticulum. *J. Gen. Physiol.* 104:857–883.

Harvey, A. L., and A. J. Anderson. 1985. Dendrotoxins: snake toxins that block potassium channels and facilitate neurotransmitter release. *Pharmacol. & Ther.* 31:33–55.

Heinemann, S. H., and F. J. Sigworth. 1990. Open channel noise. V. Fluctuating barriers to ion entry in gramicidin A channels. *Biophys. J.* 57:499–514.

Heinemann, S. H., and F. J. Sigworth. 1991. Open channel noise. VI. Analysis of amplitude histograms to determine rapid kinetic parameters. *Biophys. J.* 60:577–587.

Heinemann, S. H., and F. J. Sigworth. 1993. Fluctuations of ionic currents and ion channel proteins. *In* Thermodynamics of Membrane Receptors and Channels. M. B. Jackson, editor. CRC Press, Boca Raton, FL. 407–422.

Hill, J. A., R. Coronado, and H. C. Strauss. 1989. Potassium channel of cardiac sarcoplasmic reticulum is a multi-ion channel. *Biophys. J.* 55:35–46.

Hill, J. A., R. Coronado, and H. C. Strauss. 1990. Open channel subconductance of K^+ channel from cardiac sarcoplasmic reticulum. *Am. J. Physiol.* 258:H159–H164.

Hille, B. 1992. Ionic Channels of Excitable Membranes. 2nd edition, Sinauer Associates, Sunderland MA.

Hurst, R. S., A. E. Busch, M. P. Kavanaugh, P. B. Osborne, R. A. North, and J. P. Adelman. 1991. Identification of amino acid residue involved in dendrotoxin block of voltage-dependent potassium channels. *Mol. Pharmacol.* 40:572–576.

Isacoff, E. Y., Y. N. Jan, and L. Y. Jan. 1991. Putative receptor for the cytoplasmic inactivation gate in the *Shaker* K^+ channel. *Nature (Lond.).* 353:86–90.

Jiang, C., and G. G. Haddad. 1994. A direct mechanism for sensing low oxygen levels by central neurons. *Proc. Natl. Acad. Sci. USA.* 91:7198–7201.

Labarca, P. P., and C. Miller. 1981. A K^+-selective, three-state channel from fragmented sarcoplasmic reticulum of frog leg muscle. *J. Membr. Biol.* 61:31–38.

Latorre, R., P. Labarca, and D. Naranjo. 1992. Surface charge effects on ion conduction in ion channels. *Methods Enzymol.* 207: 471–501.

Läuger, P. 1983. Conformational transitions of ionic channels. *In* Single Channel Recording. B. Sakmann and E. Neher, editors. Plenum Publishing Corp., NY. 177–189.

Läuger, P. 1985. Ionic channels with conformational substates. *Biophys. J.* 47:581–591.

Läuger, P., W. Stephan, and E. Frehland. 1980. Fluctuations of barrier structure in ionic channels. *Biochim. Biophys. Acta.* 602:167–180.

Lindsay, A. R. G., A. Tinker, and A. J. Williams. 1994. How does ryanodine modify ion handling in the sheep cardiac sarcoplasmic reticulum Ca^{2+}-release channel? *J. Gen. Physiol.* 104:425–447.

Lucchesi, K., and E. Moczydlowski. 1990. Subconductance behavior in a maxi Ca^{2+}-activated K^+ channel induced by dendrotoxin-I. *Neuron.* 2:141–148.

Lucchesi, K. J., and E. Moczydlowski. 1991. On the interaction of bovine pancreatic trypsin inhibitor with maxi Ca^{2+}-activated K^+ channels. *J. Gen. Physiol.* 97:1295–1319.

Lukacs, G. L., and E. Moczydlowski. 1990. A chloride channel from lobster walking leg nerves. Characterization of single-channel properties in planar bilayers. *J. Gen. Physiol.* 96:707–733.

Marshall, D. L., and A. L. Harvey. 1990. Re-examination of the protease inhibitor activities of the dendrotoxins from mamba venoms. *Toxicon.* 28:157–158.

Marshall, D. L., and A. L. Harvey. 1992. Protease inhibitor homologues of dendrotoxin do not bind to dendrotoxin acceptors on synaptosomal membranes or facilitate neuromuscular transmission. *Biol. Chem. Hoppe-Seyler.* 373:707–714.

Matteson, D. R., and R. P. Swenson, Jr. 1986. External monovalent cations that impede the closing of K channels. *J. Gen. Physiol.* 87: 795–816.

McManus, O. B., A. L. Blatz, and K. L. Magleby. 1987. Sampling, log binning, fitting, and plotting durations of open and shut intervals from single channels and the effect of noise. *Pflügers Archiv Eur. J. Physiol.* 410:530–533.

McManus, O. B., and Magleby, K. L. 1988. Kinetic states and modes of single large conductance calcium activated potassium channels in cultured rat skeletal muscle. *J. Physiol.* 402:79–120.

Miller, C., E. Moczydlowski, R. Latorre, and M. Phillips. 1985. Charybdotoxin, a protein inhibitor of single Ca^{2+}-activated K^+ channels from mammalian skeletal muscle. *Nature (Lond.).* 313: 316–318.

Miller, C., R. Latorre, and I. Reisin. 1987. Coupling of voltage-dependent gating and Ba^{2+} block in the high-conductance, Ca^{2+}-activated K^+ channel. *J. Gen. Physiol.* 90:427–449.

Milne, R. K., G. F. Yeo, B. W. Madsen, and R. O. Edeson. 1989. Estimation of single channel kinetic parameters from data subject to limited time resolution. *Biophys. J.* 55:673–676.

Mironov, S. L. 1992. Conformational model for ion permeation in membrane channels: a comparison with multi-ion models and applications to calcium channel permeability. *Biophys. J.* 63:485–496.

Moczydlowski, E., and L. Schild. 1994. Unitary properties of the batrachotoxin-trapped state of voltage-sensitive sodium channels. *In* Handbook of Membrane Channels. C. Peracchia, editor. Academic Press, NY. 137–160.

Moczydlowski, E., G. W. J. Moss, and K. J. Lucchesi. 1992. Bovine pancreatic trypsin inhibitor as a probe of large conductance Ca^{2+}-activated K^+ channels at an internal site of interaction. *Biochem. Pharmacol.* 43:21–28.

Moss, G. W. J., and E. G. Moczydlowski. 1993. Energy barrier fluctuations in a Ca-activated K-channel revealed by analysis of subconductance states induced by BPTI and dendrotoxin-I. *Biophys. J.* 64:A3.

Moss, G. W. J., and E. G. Moczydlowski. 1995. General effect of rapid fluctuations on practical measurements of unitary channel current as determined by computer simulation. *Biophys. J.* 68: A371.

Nakazawa, K., and P. Hess. 1993. Block by calcium of ATP-activated channels in pheochromocytoma cells. *J. Gen. Physiol.* 101:377–392.

Neyton, J., and M. Pelleschi. 1991. Multi-ion occupancy alters gating in high-conductance, Ca^{2+}-activated K^+ channels. *J. Gen. Physiol.* 97:641–665.

Nowycky, M. C., A. P. Fox, and R. W. Tsien. 1985. Three types of neuronal calcium channels with different calcium agonist sensitivity. *Nature (Lond.).* 316:440–443.

Ogden, D. C., and D. Colquhoun. 1985. Ion channel block by acetylcholine, carbachol and suberyldicholine at the frog neuromuscular junction. *Proc. R. Soc. Lond. B Biol. Sci.* 225:329–355.

Oiki, S., R. E. Koeppe, and O. S. Andersen. 1992. A dipolar amino acid substitution induces voltage-dependent transitions between two stable conductance states in gramicidin channels. *Biophys. J.* 62:28–30.

Patlak, J. B. 1993. Measuring kinetics of complex single ion channel data using mean-variance histograms. *Biophys. J.* 65:29–42.

Press, W. H., B. P. Flannery, S. A. Teukolsky, and W. T. Vetterling. 1986. Numerical recipes, the art of scientific computing. Cambridge University Press, Cambridge, UK.

Richard, E. A., and C. Miller. 1990. Steady-state coupling of ion-channel conformations to a transmembrane ion gradient. *Science (Wash. DC).* 247:1208–1210.

Root, M. J., and R. MacKinnon. 1994. Two identical noninteracting sites in an ion channel revealed by proton transfer. *Science (Wash. DC).* 265:1852–1856.

Schild, L., and E. Moczydlowski. 1994. Permeation of Na^+ through open and Zn^{2+}-occupied conductance states of cardiac sodium channels modified by batrachotoxin: exploring ion-ion interactions in a multi-ion channel. *Biophys. J.* 66:654–666.

Schurholz, T., L. Dioczik, and E. Neumann. 1993. Single-channel analysis of the anion channel-forming protein from the plant pathogenic bacterium *Clavibacter michiganese ssp. nebraskense. Biophys. J.* 64:58–67.

Shen, K.-Z., A. Lagrutta, N. W. Davies, N. B. Standen, J. P. Adelman, and R. A. North. 1994. Tetraethylammonium block of slowpoke calcium-activated potassium channels expressed in *Xenopus* oocytes: evidence for tetrameric channel formation. *Pflügers Arch. Eur. J. Physiol.* 426:440–445.

Sigworth, F. J. 1980. The variance of sodium current fluctuations at the node of Ranvier. *J. Physiol.* 307:97–129.

Sigworth, F. J. 1985. Open channel noise. I. Noise in acetylcholine receptor currents suggests conformational fluctuations. *Biophys. J.* 47:709–720.

Sigworth, F. J., and S. M. Sine. 1987. Data transformations for improved display and fitting of single-channel dwell time histograms. *Biophys. J.* 52:1047–1054.

Skarzynski, T. 1992. Crystal structure of α-dendrotoxin from the green mamba venom and its comparison with the structure of bovine pancreatic trypsin inhibitor. *J. Mol. Biol.* 224:671–683.

Stühmer, W., J. P. Ruppersberg, K. H. Schroter, B. Sakmann, M. Stocker, K. P. Giese, A. Perschke, A. Baumann, and O. Pongs. 1989. Molecular basis of functional diversity of voltage-gated potassium channels in mammalian brain. *EMBO (Eur. Mol. Biol. Organ.) J.* 8:3235–3244.

Swenson, R. P., and C. M. Armstrong. 1981. K^+ channels close more slowly in the presence of external K^+ and Rb^+. *Nature (Lond.).* 291:427–429.

Taglialatela, M., J. A. Drewe, G. E. Kirsch, M. DeBiasi, H. A. Hartman, and A. M. Brown. 1993. Regulation of K^+/Rb^+ selectivity and internal TEA blockade by mutations at a single site in K^+ pores. *Pflügers Arch. Eur. J. Physiol.* 423:104–112.

Tomlins, B., A. J. Williams, and R. A. P. Montgomery. 1984. The characterization of a monovalent cation-selective channel of mammalian cardiac muscle sarcoplasmic reticulum. *J. Membr. Biol.* 80:191–199.

Toro, L., E. Stefani, and R. Latorre. 1992. Internal blockade of a Ca^{2+}-activated K^+ channel by Shaker B inactivating "ball" peptide. *Neuron.* 9:237–245.

Tyerman, S. D., B. R. Terry, and G. P. Findlay. 1992. Multiple conductances in the large K^+ channel from *Chara corallina* shown by a transient analysis method. *Biophys. J.* 61:736–749.

Vergara, C., and R. Latorre. 1983. Kinetics of Ca^{2+}-activated K^+ channels from rabbit muscle incorporated into planar bilayers: evidence for a Ca^{2+} and Ba^{2+} blockade. *J. Gen. Physiol.* 82:543–568.

Villarroel, A. 1989. Mechanism of ion conduction in the large calcium activated potassium channel. Ph.D. Thesis. University of California, Los Angeles, CA.

Villarroel, A., and G. Eisenman. 1987. Surface charage in a barrier model can explain the low conductance behavior of the Ca^{2+}-activated K^+ channel. *Biophys. J.* 51:546*a* (Abstr.).

Wang, G., M. Dugas, B. I. Armah, and P. Honerjäger. 1990. Sodium channel comodification with full activator reveals veratridine reactions dynamics. *Mol. Pharmacol.* 37:144–148.

Welsh, M. J., and C. M. Liedtke. 1986. Chloride and potassium channels in cystic fibrosis airway epithelia. *Nature (Lond.).* 322: 467–470.

Wonderlin, W. F., and R. J. French. 1991. Ion channels in transit: voltage-gated Na and K channels in axoplasmic organelles of the squid *Loligo pealei. Proc. Natl. Acad. Sci. USA.* 88:4391–4395.

Wonderlin, W. F., A. Finkel, and R. J. French. 1990*a*. Optimizing planar bilayer single-channel recordings for high resolution with rapid voltage steps. *Biophys. J.* 58:289–297.

Wonderlin, W. F., R. J. French, and N. J. Arispe. 1990*b*. Recording and analysis of currents from single ion channels. *In* Neuromethods, Vol. 14: Neurophysiological Techniques: Basic Methods and Concepts. A. A. Boulton, G. B. Baker, and C. H. Vanderwolf, editors. The Humana Press, Clifton, NJ. 35–142.

Yellen, G. 1984. Ionic permeation and blockade in Ca^{2+}-activated K^+ channels of bovine chromaffin cells. *J. Gen. Physiol.* 84:157–186.